Corrigendum

Mechanics of limb bone loading during terrestrial locomotion in river cooter turtles (*Pseudemys concinna*)

M. T. Butcher and R. W. Blob

10.1242/jeb.021329

The authors would like to correct two errors published in *J. Exp. Biol.* **211**, 1187-1202.

First, in three places in the article, the reported value of yield stress in torsion for the femur of *Pseudemys concinna* was too high by a factor of 2. This error occurred in Table 5, in the second paragraph of the Results section entitled 'Mechanical properties and safety factor calculations' (p. 1196) and in the first paragraph of the Discussion section entitled 'Femoral safety factors in turtles: mechanical basis and implications for the evolution of limb bone design' (p. 1199). The correct value is 39.1±3.3 MPa, which is 35% lower than values for bovine and human bone (Currey, 2002), rather than 40% higher as reported (p. 1196 and p. 1199). All calculations of *in vivo* bending and shear stress and of safety factors in bending were unaffected by this error, but the mean safety factor to yield in shear reported in the Summary (p. 1187), Table 5 and the text on p. 1196 and p. 1199 should be corrected from 6.3 to 3.1, and the worst-case estimate of safety factor to yield in shear reported in the text on p. 1196 should be corrected from 3.1 to 1.6. A corrected Table 5 is presented below.

Table 5. Mechanical properties and safety factors for femora and tibiae of *P. concinna*

		Bending			Torsion	
Bone	*N*	Yield stress (MPa)	Safety factor mean	*N*	Yield stress (MPa)	Safety factor mean
Femur	3	305.9±66.3	13.9	3	39.1±3.3	3.1
Tibia	4	143.4±22.1	6.5*	–	–	–

*Tibial safety factor calculated from tibia yield stress and average peak locomotor stresses of the femur.
Yield stress values are means ± s.e.m.

Although mean femoral safety factors for shear in the turtle *P. concinna* are now moderately lower than those previously reported for lizards and crocodilians [4.9 and 5.4, respectively (Blob and Biewener, 1999)], rather than the moderately higher value (6.3) originally reported, values for all three of these ectothermic lineages are still higher than those for the humerus of flying pigeons [1.9 (Biewener and Dial, 1995)]. These comparisons continue to suggest, as originally noted, greater protection against torsional limb bone failure in quadrupedal reptiles than in other lineages where torsion is prominent. Moreover, they further emphasize the significance of torsion as a femoral loading regime in turtles and the impact of variation in bone mechanical properties on skeletal functional capacity, as originally proposed.

Second, in the PDF and print versions of the article, the reference cited on p. 1191 as (Stein, 2003) also contained errors and should be amended to Stein (2005) as follows:

Stein, P. S. (2005). Neuronal control of turtle hindlimb motor rhythms. *J. Comp. Physiol. A* **191**, 213-229.

In the full-text online version of this article, the reference has been corrected to allow linking to Medline.

The authors apologize for these errors but assure readers that, with the clarifications noted above, the results and conclusions of the original paper remain unchanged.

REFERENCES

Biewener, A. A. and Dial, K. P. (1995). *In vivo* strain in the humerus of pigeons (*Columba livia*) during flight. *J. Morph.* **225,** 61-75.
Blob, R. W. and Biewener, A. A. (1999). *In vivo* locomotor strain in the hindlimb bones of *Alligator mississippiensis* and *Iguana iguana*: implications for the evolution of limb bone safety factor and non-sprawling limb posture. *J. Exp. Biol.* **202,** 1023-1046.
Currey, J. D. (2002). *Bones. Structure And Mechanics.* Princeton, NJ: Princeton University Press.

The Journal of Experimental Biology 211, 1187-1202
Published by The Company of Biologists 2008
doi:10.1242/jeb.012989

Mechanics of limb bone loading during terrestrial locomotion in river cooter turtles (*Pseudemys concinna*)

Michael T. Butcher and Richard W. Blob*
Department of Biological Sciences, 132 Long Hall, Clemson University, Clemson, SC 29634, USA
*Author for correspondence (e-mail: rblob@clemson.edu)

Accepted 1 February 2008

SUMMARY

Studies of limb bone loading during terrestrial locomotion have focused primarily on birds and mammals. However, data from a broader functional and phylogenetic range of species are critical for understanding the evolution of limb bone function and design. Turtles are an interesting lineage in this context. Although their slow walking speeds and robust limb bones might lead to low locomotor forces and limb bone stresses similar to other non-avian reptiles, their highly sprawled posture could produce high bending loads, leading to high limb bone stresses similar to those of avian and mammalian species, as well as high torsion. To test between these possibilities, we evaluated stresses experienced by the femur of river cooter turtles (*Pseudemys concinna*) during terrestrial walking by synchronizing measurements of three-dimensional joint kinematics and ground reaction forces (GRFs) during isolated hindlimb footfalls. Further, we evaluated femoral safety factors for this species by comparing our locomotor stress calculations with the results of mechanical property tests. The net GRF magnitude at peak tensile bone stress averaged 0.35 BW (body weight) and was directed nearly vertically for the middle 40–65% of the contact interval, essentially orthogonal to the femur. Peak bending stresses experienced by the femur were low (tensile: 24.9±9.0 MPa; compressive: –31.1±9.1 MPa) and comparable to those in other reptiles, yet peak shear stresses were higher than those in other reptiles, averaging 13.7±4.2 MPa. Such high torsion is present despite cooters lacking a large tail, a feature that has been hypothesized to contribute to torsion in other reptiles in which the tail is dragged along the ground. Comparison of femoral stresses to measurements of limb bone mechanical properties in cooters indicates safety factors to yield of 13.9 in bending and 6.3 in torsion, considerably higher than values typical for birds and mammals, and closer to the elevated values calculated for other reptile species. Thus, not only do turtle limb bones seem considerably 'over-designed' for resisting the loads that they encounter, but comparisons of bone loading across tetrapod lineages are consistent with the hypothesis that low limb bone loads, elevated torsion and high safety factors may be primitive features of limb bone design.

Key words: locomotion, biomechanics, kinematics, force, bone stress, safety factor, turtle.

INTRODUCTION

Tetrapod limb bones show a diverse range of shapes and designs, from the elongate bones of fast runners to the short, robust limbs of many fossorial species. A major factor commonly thought to have contributed to the diversity of limb bone form and function that has evolved across these species is variation in the mechanical loads that their bones experience (Currey, 1984; Currey, 2002; Blob, 2001; Lieberman et al., 2004). Among terrestrial tetrapods, the behavior generally thought to exert the greatest influence on the loading environment of limb bones is locomotion, because it usually imposes the largest and most frequent loads on the skeleton (Biewener, 1990; Biewener, 1993). Limb bones must resist the loads incurred during locomotion or risk failure, which, even if not fatal, could seriously impede behaviors such as resource acquisition and mating, thereby decreasing fitness. Vertebrate limb bones typically have a margin of safety against such failure and can withstand loads several times higher than those they usually experience (Alexander, 1981; Biewener, 1993; Blob and Biewener, 1999). Although high values of such safety factors could be advantageous in preventing failure, they could also be energetically costly (Diamond, 1998), potentially requiring extra bone to be not only produced and maintained, but also transported during daily activity.

The capacity of bones to resist the loads they encounter depends on two primary factors: the nature of the loads (magnitude and loading regime) and the mechanical properties of the skeletal elements. Evaluations of these factors in tetrapod limb bones, particularly loading magnitudes and regimes, have focused mainly on species of birds and mammals (e.g. Rubin and Lanyon, 1982; Biewener, 1983a; Biewener, 1983b; Biewener et al., 1983; Biewener et al., 1988; Carrano, 1998; Demes et al., 2001; Lieberman et al., 2004; Main and Biewener, 2004; Main and Biewener, 2007). These studies have found several common features in the limb bone loading of these taxa during terrestrial locomotion. First, limb bones are typically loaded in bending or axial compression (Biewener, 1990; Biewener, 1991). Torsion is generally less common among quadrupeds (Carter et al., 1980; Keller and Spengler, 1989), though it has been indicated in the limb bones of bipedal birds (Biewener et al., 1986; Carrano, 1998; Main and Biewener, 2007). Second, limb bone safety factors of birds and mammals are commonly between 2 and 4 (Alexander 1981; Biewener, 1993), with the mechanical properties of bones differing little among species (Biewener, 1982; Erickson et al., 2002). However, studies in lizards (iguanas) and crocodilians (alligators) found different patterns of bone loading from those typical in birds or mammals, with more substantial torsion but higher safety factors (up to 10.8 in bending,

5.4 in shear) that resulted from both lower magnitude loads and higher resistance to failure than found in birds and mammals (Blob and Biewener, 1999; Blob and Biewener, 2001). These findings from iguanas and alligators suggested the potential for greater diversity in tetrapod limb bone mechanics and design than avian and mammalian studies had indicated, but explanations for the differences in bone loading among these lineages were not resolved. It is possible that the high limb bone safety factors found in iguanas and alligators represent adaptations to a variety of demands placed on their limbs, ranging from low rates of bone remodeling to high variability in locomotor load (Blob and Biewener, 1999; Blob and Biewener, 2001). However, it is also possible that the loading patterns seen in iguana and alligator limb bones are simply retentions of ancestral tetrapod conditions that were not sufficiently costly to have been selected against, and from which birds and mammals have independently diverged (Blob and Biewener, 1999; Blob and Biewener, 2001).

To address such questions and evaluate the evolutionary history of tetrapod limb bone loading mechanics, data from a broader functional and phylogenetic range of species are required. In this context, turtles are a particularly interesting lineage for study. Although the phylogenetic relationship of turtles to the lepidosaur and archosaur lineages is controversial (Hedges and Poling, 1999; Rieppel and Reisz, 1999; Rieppel, 2000; Zardoya and Meyer, 2001; Rest et al., 2003; Hill, 2005), limb bone loading data from turtles would provide information from a third reptilian (*sensu* Modesto and Anderson, 2004) clade, providing additional perspective on whether loading patterns seen in iguanas and alligators are unusual to those taxa, or more broadly representative of reptiles in general. In addition, several distinctive features of turtle morphology and behavior lead to questions about how their limb bones might be expected to be loaded. For example, with their body largely surrounded by a heavy, bony shell, turtles are generally slow and can only walk (Walker, 1971; Zug, 1971; Claussen et al., 2004), with peak ground reaction forces (GRFs) of only 0.5 BW (body weight) acting on a single hindlimb during terrestrial locomotion (Jayes and Alexander, 1980). These features could lead to expectations of low limb bone loading magnitudes. However, turtles typically have short, robust limb bones (Walker, 1973) that would be expected to provide considerable structural reinforcement against locomotor loads. Could turtle limb bones be even more over-built than those of other reptiles? Alternatively, might the robust bones of turtles help protect against unexpectedly high limb bone stresses, potentially resulting from a highly sprawled posture (Walker, 1971; Zug, 1971) that orients the limb at a large angle from the GRF and induces high bending loads (Biewener, 1989; Biewener, 1990)? A second distinctive feature of turtles compared with most reptiles, reduction of the tail (Willey and Blob, 2004), might have further implications for the dominant loading regime their limb bones would experience. Although the two quadrupedal taxa using non-parasagittal locomotion in which limb bone loads have been examined (iguanas and alligators) both showed high torsion in their hindlimb bones (Blob and Biewener, 1999; Blob and Biewener, 2001), recent studies have suggested that such torsional limb bone loading was largely a consequence of these species dragging a heavy tail, and that torsion would be limited in sprawling species that did not tail-drag (Willey et al., 2004; Reilly et al., 2005). Because the tails of most turtle species do not touch the ground during terrestrial walking, but turtles still use a highly sprawled limb posture, loading data from turtle limb bones would provide an important test of the prevalence of torsion as a loading regime in tetrapod limb bones.

To examine these questions about the mechanics of limb bone loading in turtles, we evaluated the stresses developed during terrestrial walking in the femur of the river cooter, *Pseudemys concinna* (Le Conte), by collecting simultaneous three-dimensional kinematic and force platform data. Further, we evaluated femoral safety factors for this species by comparing our locomotor stress calculations with the results of mechanical property tests. Synchronized locomotor kinematic and force data allow analyses of joint equilibrium that give insight into external and muscular forces and moments acting on limb bones (Biewener and Full, 1992). These analyses produce indirect estimates of load magnitude, but also can substantially aid understanding of the mechanics underlying bone loading patterns (Blob and Biewener, 2001). Based on our evaluations of femoral stresses and safety factors in river cooters, we tested three hypotheses: (1) that turtles have low magnitudes of limb bone stress, more similar to lizards and alligators than to mammals and birds; (2) that turtle limb bones will show a high degree of torsional loading; and (3) that turtle limb bones have high safety factors, closer to those of lizards and alligators than to those of mammals and birds. Limited GRF data have been collected from turtles (Jayes and Alexander, 1980; Zani et al., 2005) but these studies did not apply force data to evaluate limb bone loads. Thus, our analyses of limb bone loading in turtles help to improve understanding of locomotor mechanics in a clade with a distinctive body plan, and provide an additional phylogentic context for evaluating the diversity of tetrapod limb bone design.

MATERIALS AND METHODS

Animals

Experiments were conducted on four river cooter turtles (two adult females, one adult male and one sub-adult male, body mass 0.8–3.7 kg) collected from a spillway of Lake Hartwell, Pickens County, SC, USA (SCDNR Scientific Collecting Permit 39-2006). Cooters are large, freshwater emydid turtles that spend the majority of their time in aquatic habitats, but frequently come on land to bask and nest, as well as to travel more extensive distances over land to move between bodies of water (Ernst et al., 1994). Although their femur is directed nearly horizontally in a highly sprawled posture, like other emydids and turtles in general (Walker, 1971; Zug, 1971), cooters have robust limbs and generally support the weight of the body off the ground during terrestrial walking. Turtles were housed in a greenhouse in large plastic cattle tanks (64 cm wide×147 cm long×99 cm deep), half-filled with fresh water and fitted with a re-circulating filter and dry basking ramp. Turtles were fed daily (collard or turnip greens supplemented with commercial pellets) and exposed to ambient sunlight conditions. In addition, for approximately 1 month prior to experimentation, the cooters were exercised on a motorized treadmill three times per week for 5–10 min bouts of walking at moderate speed. All experimental procedures followed Clemson University IACUC approved guidelines and protocols (AUP 50110). After the completion of force platform recordings and subsequent *in vivo* bone strain recordings (a complementary study, M.T.B. and R.W.B., manuscript in preparation), turtles were killed by an overdose of pentobarbital sodium solution (Euthasol®, Delmarva Laboratories Inc., Midlothian, VA, USA; 200 mg kg^{-1} intraperitoneal injection) and frozen for later dissection and measurement of anatomical variables and limb bone mechanical properties.

Data collection: three-dimensional kinematics and GRFs

Turtles were filmed simultaneously in lateral and posterior views at 100 Hz using a two-camera, digitally synchronized, high-speed

video system (Phantom v.4.1, Vision Research Inc., Wayne, NJ, USA) while walking over a custom-built force platform (K&N Scientific, Guilford, VT, USA). The platform was inserted between two 1.6 m segments of a wooden trackway. An aluminium frame placed over the 22 cm×17 cm surface of the platform contained a window that was fitted with an aluminium insert that was attached directly to the original platform surface. This restricted the recording surface to an 11 cm×10 cm area in the center of the platform, allowing footfalls by a single limb to be recorded. The frame and insert (recording) surface were mounted flush with the trackway surface. To prevent foot slippage during locomotor trials, the trackway surface was covered with a spray-grit coating and the force-recording surface was covered with thin rubber. Turtles were prompted to walk by tapping the shell or providing enticements such as a hide box or basking area, and were allowed to choose their own walking speed during trials. Trials consisted of filming contact of the right hindlimb with the force platform from toe-down to toe-off. To facilitate digitizing of anatomical landmarks from videos, dots of white paint were placed on the claw of the fourth digit, the metatarso-phalangeal joint, the ankle, the knee and the hip, along with three landmarks on the right side of the posterior portion of the carapace that were visible in both camera views. Temperature was maintained at 22–25°C during experiments. Turtles were allowed to rest before and after successful trials and the opportunity for periodic basking under heat lamps was provided during data collection.

Joint and landmark positions were digitized in every other frame (effective framing rate 50 Hz, ~50 frames per step) for both lateral and posterior AVI video files for each trial using a modification of the public domain NIH Image program for Macintosh, developed at the US National Institutes of Health (the modification, QuickImage, was developed by J. Walker and is available at http://www.usm.maine.edu/~walker/software.html). These two sets of coordinate data were calibrated and corrected for parallax using a customized Matlab routine (v.7.2.0; The MathWorks Inc., Natick, MA, USA). QuickSAND software (available online at http://www.usm.maine.edu/~walker/software.html) was then used to fit quintic splines to the coordinate data for every trial (Walker, 1998), smoothing the data and normalizing all trials to the same duration (101 points) to facilitate comparisons. Smoothed, normalized coordinate data were then input into a second customized Matlab routine to calculate three-dimensional kinematic variables.

The force platform allowed resolution of the vertical, anteroposterior and mediolateral components of the GRF. Locomotor forces were transduced by strain gauges bonded to aluminium beams supporting the platform, with Wheatstone bridge circuits configured to allow separate recordings of vertical force from each corner of the platform (four channels, which were summed to calculate total vertical force), separate recordings of anteroposterior force from the front and back of the plate (two channels summed to calculate total anteroposterior force), and separate recordings of mediolateral force from the left and right sides of the plate (two channels summed to calculate total mediolateral force). Raw signals from the eight platform channels were output to conditioning bridge amplifiers (12-bridge, 8-channel amplifier; K&N Scientific), sampled through an A/D converter (model PCI-6031E; National Instruments, Austin, TX, USA) at a rate of 5000 Hz and saved to computer using a customized data acquisition program written in LabVIEW (v.6.1; National Instruments). Amplifier gains for each data channel were adjusted appropriately for the body mass of each turtle to allow more sensitive resolution of GRFs. Force calibrations in all three dimensions were performed daily and verified a linear response of the force platform to loads over the range of forces sampled. Cross-talk between force channels was negligible. The natural, unloaded frequencies of the platform were 190 Hz in all three directions, sufficiently greater than the stride frequencies of the animals studied (~1 Hz) to avoid confounding the signal produced by the GRF.

Force and video records were synchronized by pressing a trigger that illuminated an LED visible in the video frame and simultaneously produced a 1.5 V pulse visible in force records. Using a customized Matlab routine, raw force records from the period of foot contact were calibrated to Newtons and summed as appropriate to produce single traces for the three force components (vertical, anteroposterior and mediolateral). QuickSAND software was then used to fit quintic splines (Walker, 1998) to the force traces, smoothing the data and interpolating the traces to the same number of points (101) as the limb position coordinate data. The point of application of the GRF was initially calculated as half the distance between the toe and the ankle; as the heel lifted from the force platform, the point of application was recalculated for each frame as half the distance between the toe and the most posterior part of the foot in contact with the platform (Blob and Biewener, 2001). This method was chosen for consistency with methods previously used for force platform analyses of bone loading in reptiles (Blob and Biewener, 2001). By the end of support the GRF was applied at the toe, reflecting an anterior shift in the GRF typical during stance phase (Carrier et al., 1994).

Isolated steps of the right hindlimb (N≈20 per animal) were selected for analysis; steps in which the right forelimb had overlapping contact on the force platform were excluded. Animal speed for each trial was calculated (m s^{-1}) by differentiating the cumulative displacement of a shell landmark (medial edge of the marginal scute just anterior to the hip joint) in QuickSAND, and then normalized to carapace length s^{-1} for comparisons among individuals. After synchronization of force and limb position data, calculations of GRF components in particular directions and joint moments due to the GRF were performed in a customized Matlab routine, ultimately allowing evaluation of femoral stresses (see below). Inertial and gravitational moments about the hindlimb joints were assumed to be negligible in our analyses because they are typically small relative to the moments produced by the GRF during stance (Alexander, 1974; Biewener and Full, 1992).

Bone stress analyses

To simplify analyses of stresses in the femur, forces acting on the hindlimbs of turtles were resolved into a frame of reference defined by the anatomical planes of the limb segments (Fig. 1B) following the designations for sprawling animals previously outlined (Blob and Biewener, 2001). Briefly, the anteroposterior plane (AP) was defined as the plane including the long axes of the tibia and femur. The dorsoventral plane (DV) was defined as the plane including the long axis of the femur that is perpendicular to the AP. The mediolateral (ML) plane was defined as the plane including the long axis of the tibia that is perpendicular to the AP. Thus, the knee and ankle joints flex and extend within the anatomical AP plane. Following this convention, the direction of a motion or force is not the same as the plane in which the motion or force occurs; for example, a dorsally directed force (tending to abduct the femur) would lie within the AP plane (Blob and Biewener, 2001).

Details of calculations and equations involved in bone stress analyses closely followed those previously published for iguanas

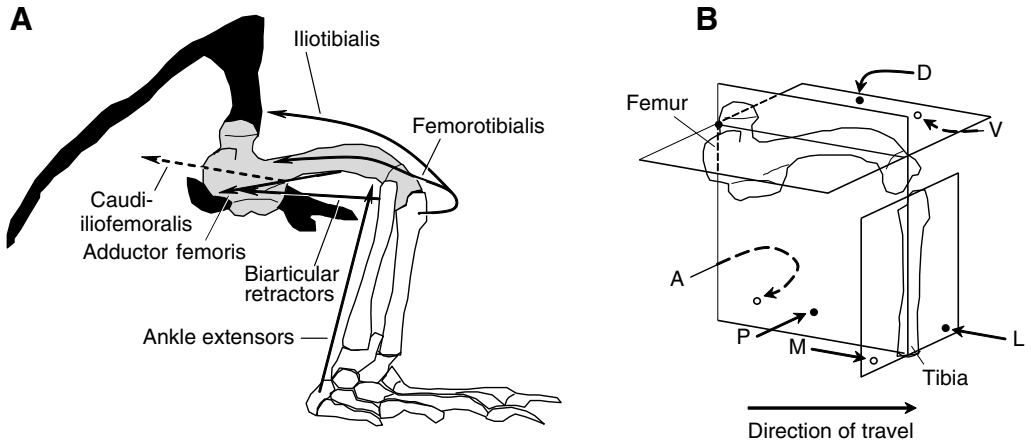

Fig. 1. (A) Outline sketch (right lateral view) of the hindlimb skeleton of *Pseudemys concinna* illustrating the lines of action of the major muscle groups contributing to stresses in the femur during the stance phase of terrestrial locomotion. Pelvic girdle bones and tail vertebrae are colored black and femur is shaded grey. Some proximal hip muscles that do not span the femoral midshaft and do not contribute directly to femoral stress (e.g. puboischiofemoralis externus, ischiotrochantericus) have been omitted for clarity. Rotational forces exerted by caudi-iliofemoralis (dashed arrow) were not calculated (see text). (B) Outline sketch of the right femur and tibia (same as in A) of *P. concinna* illustrating the planes defining the anatomical frame of reference for force platform analyses. Both surfaces of the plane are labeled, with solid arrows and filled circles indicating surfaces in view and dashed arrows and open circles indicating surfaces hidden from view (i.e. surfaces that can only be seen if the planes are transparent). A, anterior; P, posterior; D, dorsal; V, ventral; L, lateral; M, medial.

and alligators (Blob and Biewener, 2001) and will only be summarized below. Femoral stresses were calculated at the bone midshaft, where bending moments are typically highest (Biewener and Taylor, 1986), based on free body diagrams of the distal half of the femur (Alexander, 1974; Biewener et al., 1983; Beer and Johnston, 1997). Thus, only forces acting on the distal half of each bone, including the GRF and forces exerted by muscles spanning the midshaft of the femur (Fig. 1, Table 1), entered directly into our calculations of peak bending stress.

To calculate estimates of muscle forces, we assumed the limb joints to be in static rotational equilibrium (Alexander, 1974; Biewener, 1983a; Biewener and Full, 1992) and, initially, that the only muscles active at a joint were those that counteract the rotational moment of the GRF. With these assumptions, muscle forces (F_m) required to maintain joint equilibrium can be calculated as:

$$F_m = R_{GRF} \times GRF / r_m , \quad (1)$$

where R_{GRF} is the moment arm of the GRF about the joint (calculated in our Matlab routine) and r_m is the moment arm of the muscles countering the GRF moment (Alexander, 1974; Biewener 1983a; Biewener, 1989). When multiple muscles were active to counteract the GRF moment at a joint, a weighted mean moment arm was calculated for the group based on the physiological cross-sectional area (PCSA) of each muscle, which was assumed to be proportional to the forces they exert (Alexander, 1974; Biewener and Full, 1992). Muscle moment arms were measured with digital

Table 1. Anatomical data from hindlimb muscles of experimental animals (*P. concinna*)

	pc04			pc05			pc07			pc08		
Muscle	*A*	θ	r_m	*A*	θ	r_m	*A*	θ	r_m	*A*	θ	r_m
Hip retractors												
Pubotibialis + FTI*	82.9	8	7.1[h], 8.1[k]	103.7	10	14.4[h], 8.3[k]	56.9	10	12.0[h], 11.7[k]	69.5	10	8.8[h], 5.5[k]
FTE	51.9	20	17.2[h], 8.4[k]	81.2	20	12.5[h], 19.0[k]	54.2	20	11.3[h], 14.4[k]	34.7	20	8.0[h], 9.6[k]
Caudi-iliofemoralis	132.5	0	9.5[h]	111.7	0	11.1[h]	62.4	0	12.9[h]	83.0	0	9.1[h]
Ischiotrochantericus	86.5	0	11.1[h]	76.1	0	9.7[h]	65.6	0	8.5[h]	37.9	0	6.4[h]
Hip adductors												
Adductor femoris	18.7	15	5.5[h]	26.7	15	12.2[h]	17.6	15	8.5[h]	12.4	15	5.9[h]
PIFE	73.6	0	5.6[h]	185.2	0	9.9[h]	115.8	0	7.4[h]	74.1	0	6.7[h]
Knee extensors												
Iliotibialis	18.3	15	4.2[k]	28.2	10	4.2[k]	13.3	12	2.9[k]	12.9	12	3.5[k]
Femorotibialis	67.4	0	5.1[k]	89.1	0	2.7[k]	63.0	0	3.1[k]	56.6	0	2.5[k]
Ankle extensors												
Gastrocnemius (lateral)	12.1	0	6.4[a], 5.9[k]	21.4	0	3.4[a], 9.0[k]	20.9	0	2.7[a], 7.2[k]	9.5	0	3.6[a], 4.9[k]
Gastrocnemius (medial)	19.4	0	2.9[a]	19.4	0	3.2[a]	5.9	0	3.7[a]	9.8	0	3.2[a]
FDL	43.6	0	3.5[a], 3.8[k]	56.1	0	2.7[a], 5.7[k]	38.1	0	3.1[a], 4.1[k]	25.8	0	3.0[a], 3.6[k]
Pronator profundus	50.7	0	2.3[a]	39.1	0	4.1[a]	61.3	0	3.1[a]	14.4	0	2.0[a]

A, cross-sectional area of muscle (mm^2); θ, angle between the muscle and the long axis on bone (degrees); r_m, moment arm of the muscle (mm) about the joint indicated by the superscript letter (h, hip; k, knee; a, ankle); PIFE, puboishiofemoralis externus; FTI, flexor tibialis internus; FTE, flexor tibialis externus; FDL, flexor digitorum longus.

*Measurements of pubotibialis and FTI were combined in analyses due to their close association.

calipers during specimen dissections with the limbs held in a midstance position; PCSAs (Table 1) were calculated following published protocols (Biewener and Full, 1992).

Our model of muscle forces placing stress on the femur included extensors of the ankle, flexors and extensors of the knee, and femoral adductors and retractors (Fig. 1A; see Appendix). Because the GRF exerts a flexor moment at the ankle for almost all of stance (see Results), only ankle extensor muscles must be considered in our model, allowing straightforward calculation of the forces they exert. Anatomical relationships (Walker, 1973) indicate that four muscles are in positions suitable to extend the ankle (i.e. plantarflex the foot): lateral gastrocnemius, medial gastrocnemius, flexor digitorum longus and pronator profundus. Activation data are not available for any of these muscles in turtles, but electromyography (EMG) data support the gastrocnemius as an ankle extensor in other reptiles (Reilly, 1995; Reilly and Blob, 2003). All four muscles were considered to be active as ankle extensors in this study.

Evaluation of the forces exerted by muscles spanning the femur is complicated because multiple muscle groups cross the hip and knee joints. Details of our model, modified from one previously published for iguanas and alligators (Blob and Biewener, 2001), are presented in the Appendix, but it is based on the following key features. (i) Muscles are assumed to act in the same anatomical plane throughout contact. (ii) Five muscles (pubotibialis, flexor tibialis internus, flexor tibialis externus, caudi-iliofemoralis and ischiotrochantericus) are in positions to contribute to retractor moments at the hip, but only the first three of these (i.e. biarticular retractors; Fig. 1A) span the length of the femur. Moreover, although EMG data from walking turtles indicate that some of these muscles are active during stance (Earhart and Stein, 2000; Gillis and Blob, 2001; Stein, 2003; Blob et al., 2008), our force platform recordings (see Results) indicate that the GRF also has a retractor moment during stance, preventing us from estimating the contributions of these muscles to femoral stress. This may lead to some underestimation of AP stress in our calculations, but several factors suggest this underestimation is minimized (see Appendix). (iii) Hip adductor muscles (adductor femoris and puboischiofemoralis externus) counter the abductor moment of the GRF at the hip, with adductor femoris spanning the femoral midshaft, bending it to place its ventral cortex in compression. (iv) Knee extensors (iliotibialis and femorotibialis) on the dorsal surface of the femur counter the combined knee flexor moments of the GRF and ankle extensors that span the knee (Blob and Biewener, 2001). The bending moment induced by the knee extensors opposes that induced by hip adductors, placing the dorsal femoral cortex in compression. Because muscles crossing the hip and knee have opposing actions there is no unique solution to muscle force calculations; however, the model we applied in this study accounts for the known co-activation of antagonist muscle groups to the extent possible. Muscle force calculations were made for each of the 101 time increments for each trial using the customized Matlab analysis routine.

Muscular contributions to femoral torsion (i.e. shear stresses) were not estimated. The primary femoral rotator in cooters, the caudi-iliofemoralis, inserts ventrally on the femur and, thus, would augment the rotational moment imposed by the GRF. Therefore, calculations of the rotational force exerted by this muscle based on equilibrium equations cannot be made without further assumptions about the activity of antagonist muscles. Rather than make such assumptions, the torsional stress induced by the GRF alone was calculated as a minimum estimate (Blob and Biewener, 2001).

After calculating estimates of muscle force, bending moments and axial and bending stresses were calculated following published methods and equations (Biewener, 1983a; Biewener and Full, 1992; Beer and Johnston, 1997) with modifications for three-dimensional stress analysis (Blob and Biewener, 2001). Anatomical measurements of linear and angular variables (Table 2) were measured from magnified digital photographs of the femur of each turtle. Cross-sectional anatomical variables (cross-sectional area, second moments of area, polar moment of area; Table 2) were calculated from digital photographs of midshaft sections cut from each bone, traced in Microsoft Powerpoint and saved as JPEG files, then input into a customized analysis macro for NIH Image (Lieberman et al., 2003). Bending moments and stresses were calculated in the perpendicular DV and AP directions (Blob and Biewener, 2001), and accounted for bending induced by axial forces due to the moment arm of bone curvature, r_c (Biewener 1983a; Biewener, 1983b). The magnitude of net bending stress at the femoral midshaft was calculated as the vector sum of bending stresses in the perpendicular DV ($\sigma_{b/DV}$) and AP ($\sigma_{b/AP}$) directions (Blob and Biewener, 2001), allowing the orientation of peak bending stress to be calculated as:

$$\alpha_{b/net} = \tan^{-1}(\sigma_{b/DV}/\sigma_{b/AP}) , \quad (2)$$

where $\alpha_{b/net}$ is the angular deviation of peak stress from the AP axis. The net neutral axis of bending is perpendicular to this axis. Net longitudinal stresses at the points of peak tensile and compressive bending were then calculated as the sum of axial and bending stresses. Torsional stress (τ) due to the GRF was calculated as:

$$\tau = T(y_t/J) , \quad (3)$$

where T is the torsional moment applied to the bone by the GRF (determined from the magnitude of the resultant GRF and its orthogonal distance from the long axis of the femur), y_t is the distance from the centroid of the bone to its cortex, and J is the polar moment of area (Wainwright et al., 1976). For each animal, y_t was calculated as the average of the y values from the perpendicular anatomical directions (Table 2).

Table 2. Anatomical data from femora of experimental animals (*P. concinna*)

Measurement	pc04	pc05	pc07	pc08
Length (mm)	51.9	66.9	57.1	40.5
A (mm^2)	16.5	17.1	10.7	6.0
$r_{c(AP)}$ (mm)	–1.1	–0.5	–0.4	–0.9
$r_{c(DV)}$ (mm)	1.4	1.7	1.6	1.3
y_{AP} (mm)	1.9	1.9	1.8	1.6
y_{DV} (mm)	2.8	2.3	2.3	1.8
I_{AP} (mm^4)	24.2	57.6	24.9	7.9
I_{DV} (mm^4)	18.2	38.4	18.9	6.3
J (mm^4)	42.4	96.0	43.7	14.2

In subscript notations, AP denotes the anatomical anteroposterior direction for the femur, and DV denotes the anatomical dorsoventral direction for the femur; A, cross-sectional area of bone; r_c, moment arm due to bone curvature; y, distance from neutral axis to cortex; I, second moment of area; J, polar moment of area. Curvature sign conventions for AP: positive, concave posterior; negative, concave anterior; curvature sign conventions for DV: positive, concave ventral; negative, concave dorsal.

Mechanical property testing and limb bone safety factors

Mechanical properties of cooter hindlimb bones were evaluated in three-point bending and torsion. Whole limb bones were extracted from frozen specimens after thawing. To avoid introducing surface flaws onto the bones, soft tissue was firmly rubbed from bone diaphyses with a saline-soaked cotton-tipped applicator. Hydration

of the bones was maintained with saline solution after removal of soft tissue.

Whole bones (N=3 femora, N=4 tibiae) were loaded to failure in bending using an Instron (Norwood, MA, USA) model 4502 screw-driven, uniaxial materials testing machine fitted with a 10 kN load cell sensitive to 0.05 N. Anvils of the loading jig were positioned to provide a gauge length of 0.025 m or 0.030 m, depending on bone length. Bones were mounted in the jig so that the dorsal (femur) or anterior (tibia) surface was loaded in tension, consistent with patterns from preliminary *in vivo* strain recordings showing tension on the anterodorsal surface of the femur at peak strain (Espinoza and Blob, 2004; Cirilo et al., 2005) and providing a stable seating of the bones between the anvils. Cortical bone strains were recorded during bending tests using three single-element strain gauges (type FLK-1-11, Tokyo Sokki Kenkyujo Co., Tokyo, Japan) attached to the midshaft (Blob and Biewener, 1999). For femora, gauges were mounted on the anterior, anterodorsal and posterodorsal surfaces; for tibiae, gauges were mounted on the anterior, medial and lateral surfaces. Attachment sites were cleaned by light, wet sanding (600 grit sandpaper wetted with saline solution) and dried with 100% ETOH. Gauges were then attached using a self-catalyzing cyanoacrylate adhesive, with all gauges aligned within 5° of the long axis of the bone. Gauge leads were soldered into a microconnector, which was plugged into a shielded cable to carry strain signals to Vishay conditioning bridge amplifiers (model 2120B; MicroMeasurements Group, Raleigh, NC, USA). Raw strain signals were sampled at 500 Hz through an A/D converter *via* LabVIEW routines (as described for GRF data) and calibrated for analysis. Applied load and displacement data were sampled at 10 Hz, and crosshead displacement rate was set at 4.5 mm min^{-1} using Instron software control, producing strain rates comparable to peak rates measured for cooters *in vivo* (Cirilo et al., 2005).

Separate whole bone specimens (N=3 femora) were tested in torsion using an Instron model 8874 servohydraulic biaxial materials testing machine fitted with a 25 kN load cell sensitive to 0.05 N. For torsional tests, two rosette strain gauges (type FRA-1-11, Tokyo Sokki Kenkyujo Co.) were attached to the midshaft of each bone (dorsal and ventral femoral surfaces) following methods for single element gauges. Bones were suspended in machined aluminium wells into which epoxy was poured to embed 15 mm of the ends of each bone. Once hardened, the embedded ends were fitted into mounting brackets in the testing jig and twisted to failure. Twisting rate was set at 3° s^{-1} (Furman and Saha, 2000) in Instron software and performed in a direction to simulate *in vivo* internal rotation. Torque and rotation data were sampled at 10 Hz using Instron software, while strain data were sampled at 500 Hz in LabVIEW.

Yield stresses in bending (σ) were calculated as:

$$\sigma = M(y/I) , \quad (4)$$

where M is the bending moment at yield, y is the distance from the neutral axis to the bone surface and I is the second moment of area in the direction of bending. Bending moments were calculated as load multiplied by the bending moment arm, which equaled half the gauge length. Values of I were determined by the same methods described for locomotor stress calculations. Yield point was identified from plots of applied bending moment *versus* maximum tensile strain as the first point where measured strain magnitude deviated from the magnitude expected based on the initial, linear slope of the curve by 200 microstrain [$\mu\epsilon$=strain$\times 10^{-6}$ (Currey, 1990)]. Yield stresses in torsion (shear stress) were calculated from eqn 3, using the value of T at the time of yield. Safety factors for the femur of *P. concinna* were calculated as the ratio of yield stress to peak locomotor stress (based on tensile loads for femoral bending and shear loads for femoral torsion). Mean safety factors were calculated using mean values of mechanical properties and mean values of peak stresses from each individual. These safety factors were pooled to find the overall pooled mean. 'Worst case' safety factors were estimated from the ratio of mean yield stress minus 2 s.d. and mean peak locomotor stress plus 2 s.d. (Blob and Biewener, 1999; Blob and Biewener, 2001) using a similar calculation as for mean safety factors. For each individual, the s.d. of peak stress was doubled and added to the value of peak stress for each trial for that individual. These adjusted peak stress values were then averaged for each individual. Worst case safety factors were calculated for each individual using these adjusted values of peak stresses and yield stress; individual worst case safety factor values were then pooled and averaged to find the overall pooled mean.

Correlations of peak tensile stress with limb loading and kinematic variables

To evaluate factors that might be correlated with high femoral loads in turtles, relationships between peak tensile stress in the femur and a variety of kinematic and force variables were determined by reduced major axis (RMA) regressions (Blob and Biewener, 1999; Blob and Biewener, 2001). RMA is the most appropriate method of regression for the evaluation of structural relationships between variables when both are subject to error (McArdle, 1988; LaBarbera, 1989). Values of focus variables were evaluated from every analyzed run for each individual at the time of peak tensile stress, and included: femoral protraction/retraction angle, femoral abduction/adduction angle, knee angle and ankle angle; magnitudes of forces (in BW) exerted by major muscle groups modeled in the bone stress analysis (femoral adductors, knee extensors and ankle extensors); moment arms of the GRF at the hip, knee and ankle (all normalized to carapace length; CL); the magnitude of the GRF (in BW) and its angle of inclination in the AP and ML directions; and forward walking speed (in CL s^{-1}). To evaluate how broadly correlations might apply across tetrapods with sprawling limb posture, regressions for the same variables were also calculated for *I. iguana*, using data from Blob and Biewener (Blob and Biewener, 2001).

RESULTS

Overview of stance phase kinematics

Cooters exhibit a diagonal sequence walk (Hildebrand, 1976) in which diagonal limb pairs contact the ground with at least one additional contralateral limb, providing a stable triangle of support (Walker, 1971). Details of limb motion and footfall timing have been described previously for species closely related to *P. concinna* (Walker, 1971; Zug, 1972). At the time of limb contact (toe-down), the femur is oriented approximately parallel to the substrate with the hip slightly abducted (mean ± s.e.m.: 8.2±0.5°; Fig. 2). The femur is also in a protracted position at toe-down (22.6±0.6°), while the tibia is oriented anteriorly (i.e. knee anterior to ankle) by 47.7±1.4° (vertical=0°) and medially (i.e. knee medial to ankle) by –37.4±0.6° (vertical=0°). Foot posture is plantigrade, with the digits pointing forward or slightly laterally. Stance phase is dominated by femoral retraction and adduction. From toe-down to toe-off, the femur is retracted through a range of nearly 70° as the limb is adducted through a range of nearly 30°. At the knee and ankle joints, initial flexion to accommodate the weight of the body is followed by re-extension of the joints as the turtle pushes off the substrate (Fig. 2), causing the tibia to approach a nearly horizontal (90°) AP

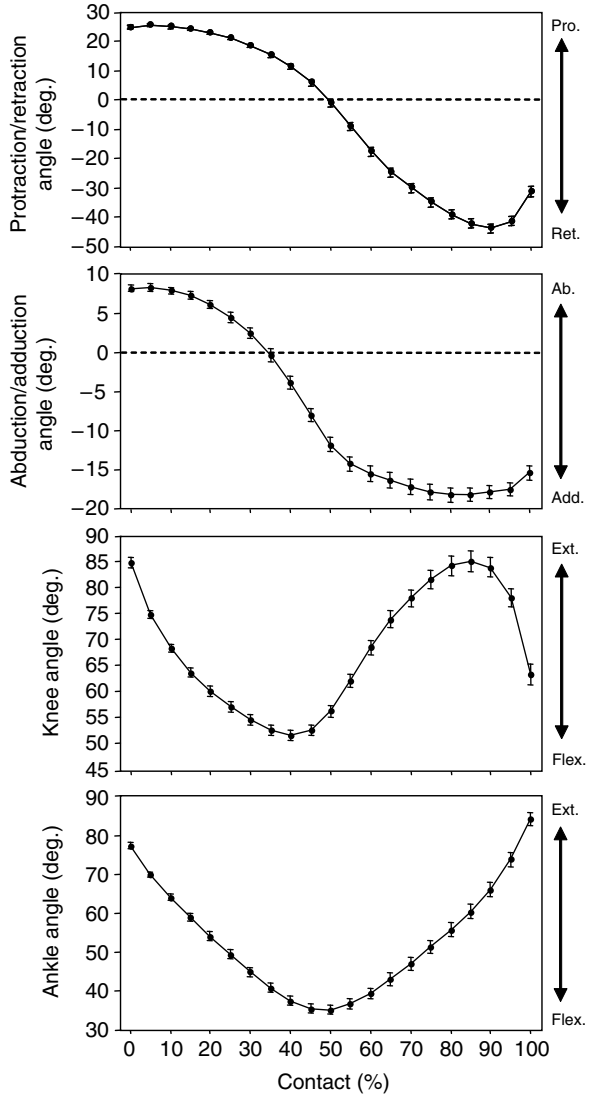

Fig. 2. Representative kinematic profiles of right hindlimb joints for river cooter turtles (*P. concinna*) during a walking step over a force platform. Top to bottom: femoral (hip) protraction (Pro.)/retraction (Ret.) angle, femoral (hip) abduction (Ab.)/adduction (Add.) angle, knee angle and ankle angle (Ext., extension; Flex., flexion). Kinematic profiles represent mean (±s.e.m.) angles averaged across all four turtles (*N*=18–21 trials per individual, 78 total steps per data point). Note that axis scales differ for these plots to provide increased resolution for smaller angles.

orientation (84.3±1.9° at 50% contact) and greatly reducing its medial deflection (–2.1° at 50% contact). Late in the contact interval (85%), the knee begins to flex again as the ankle and the metatarsals are raised off the ground (Figs 2 and 3). The tibia rotates through the horizontal plane during this interval to angles 14–16° below the horizontal, and the knee is closer to the ground than the ankle joint over the last 15% of contact. The tibia is also oriented laterally, becoming progressively more laterally directed (range 3.0–13.8°) prior to toe-off. While the ankle extends and the foot is lifted off the ground in late stance (90–100%), the femur is slightly protracted and abducted again in preparation for swing phase.

GRF magnitude and orientation

The GRF is oriented slightly posteriorly at toe-down but shifts anteriorly early in the contact interval (0–10%), remaining anteriorly directed over the remainder of stance phase (Fig. 3). The GRF is also oriented slightly medially for nearly all of stance. However, the vertical component of the GRF is considerably larger in magnitude than both the AP and mediolateral (ML) components, with the net GRF reaching peak magnitude just in advance of midstance (pooled mean: 41.0±1.1%; Table 3). Peak net GRF magnitude averaged 0.52±0.01 BW across all four turtles, with an essentially vertical orientation through the middle 40–65% of the contact interval (pooled mean at peak net GRF: AP angle, 2.9±0.8°; ML angle, –6.2±0.5°; 0°=vertical in both directions; Table 3; Fig. 3B). These magnitudes and orientations are similar to those previously reported for single hindfoot contacts in the turtle species *Geoemyda grandis* and *Testudo graeca* during walking (Jayes and Alexander, 1980).

The femur begins the step in a protracted and abducted position. As the femur is retracted throughout the contact interval, the hip joint is moving anteriorly. Thus, the femur shifts more anteriorly relative to the foot and maintains a position anterior to the point from which the net GRF vector originates for nearly the entire step. As the inclination of the GRF shifts anteriorly and medially early in the step and becomes nearly vertical prior to midstance, the net GRF vector is directed posterior to the femur for nearly all of stance (Fig. 3). As a result of this GRF orientation and the nearly horizontal orientation of the femur, the net GRF vector is oriented nearly orthogonal to the femur for most of the step, increasing to an average of 89.6±1.1° across all four turtles at peak net GRF magnitude (Table 3). Considering the near vertical orientation of the GRF vector and rotation of the femur about its long axis (counterclockwise when viewing the right femur from its proximal end; Fig. 4), femoral bending that is initially dorsoventral (i.e. about an axis close to the anatomical AP axis, with the neutral axis <45° from AP) would

Table 3. Mean peak ground reaction force data for *P. concinna*

	GRF							
Animal	Vertical (N)	AP (N)	ML (N)	Peak net GRF time (%)	net GRF (BW)	GRF femur angle (deg.)	GRF AP angle (deg.)	GRF ML angle (deg.)
pc04 (*N*=20)	11.3±0.2	–0.8±0.1	–0.7±0.1	37.8±1.6	0.57±0.01	94.3±1.0	–4.3±0.6	–3.5±0.4
pc05 (*N*=18)	16.1±0.4	0.4±0.3	–1.3±0.3	34.8±1.8	0.44±0.01	80.3±2.1	1.7±1.0	–5.0±1.2
pc07 (*N*=21)	10.4±0.3	1.8±0.3	–1.4±0.2	44.1±2.4	0.54±0.02	90.9±2.5	9.7±1.6	–8.0±1.4
pc08 (*N*=19)	3.9±0.1	0.3±0.04	–0.6±0.1	47.1±1.2	0.53±0.01	91.8±1.5	4.4±0.5	–8.1±0.6
Mean ± s.e.m.	–	–	–	41.0±1.1	0.52±0.01	89.6±1.1	2.9±0.8	–6.2±0.5

GRF femur, angle of ground reaction force to the femur; GRF AP, anteroposterior inclination angle of GRF; GRF ML, mediolateral inclination angle of GRF. Vertical=0° for GRF AP and ML angles of inclination: for GRF AP, negative angles are posteriorly directed and positive angles are anteriorly directed; for GRF ML, negative angles are medially directed. BW, body weight.
Values are means ± s.e.m. (*N*=number of steps analyzed).

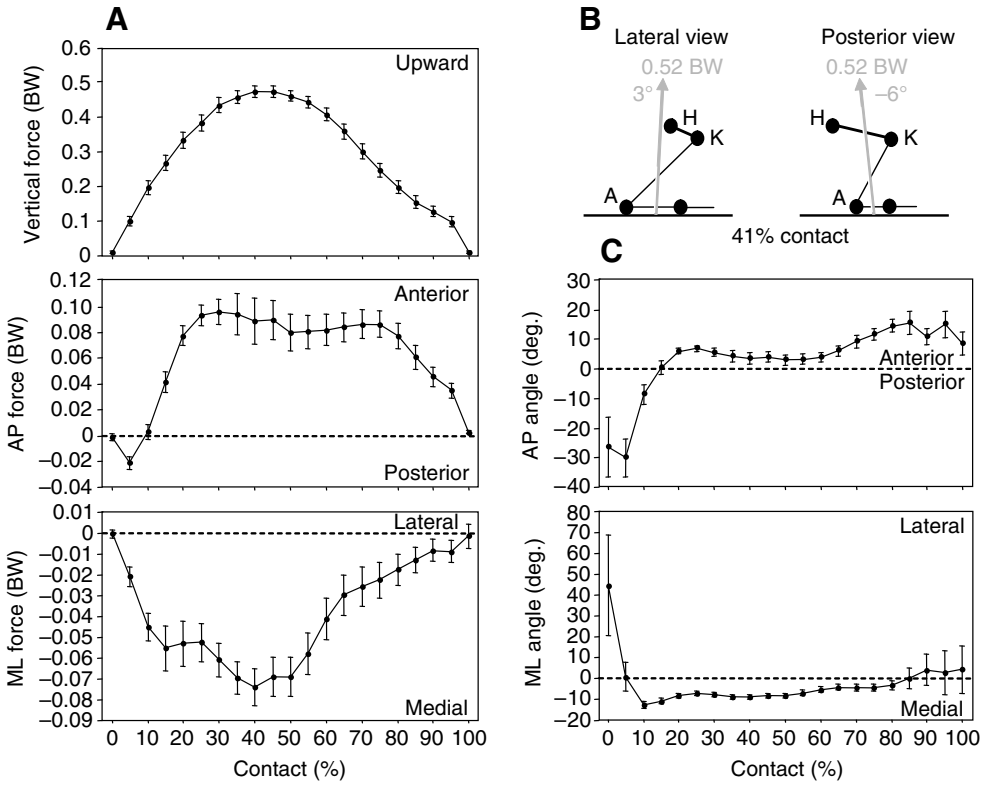

Fig. 3. Mean ground reaction force (GRF) dynamics of the right hindlimb from an individual cooter. All plots show means (±s.e.m.) over *N*=21 trials. (A) Vertical, anteroposterior (AP) and mediolateral (ML) GRF components in body weight (BW), with positive values indicating upward, anterior and lateral forces, respectively (top to bottom). Axis scales differ for these plots to provide increased resolution for the small AP and ML forces. All trials were normalized to the same duration, allowing values to be graphed against the fraction of time through the contact interval. (B) Limb segment positions at the mean time of peak net GRF (41% contact) during a representative step by *P. concinna*, with the direction and magnitude of the GRF vector illustrated. The femur is highlighted by bolder lines; note that it is foreshortened in lateral view. H, hip; K, knee; A, ankle. (C) AP and ML orientations of the net GRF vector. AP angles were determined relative to vertical at 0° (90° indicates GRF horizontal, pointing forwards; <0° indicates posteriorly directed GRF). ML angles were determined relative to vertical at 0° (positive values indicate laterally directed GRF; negative values indicate medially directed GRF).

shift toward AP bending (i.e. about an axis close to the anatomical DV axis) over the course of the step.

Moments of the GRF about hindlimb joints

For most joints, the GRF exerts moments in a consistent direction throughout stance (Fig. 4). Because of its origin anterior to the ankle, the GRF tends to dorsiflex the ankle for all of stance phase. Activity of ankle extensor muscles would be required to counter this moment. The upward orientation of the GRF posterior to the femur also leads to consistent retractor and abductor moments at the hip (Fig. 4), which would require activity by femoral protractors and adductors to maintain equilibrium. Both hip and ankle moments increase rapidly following toe-down, reaching maxima between 30% and 40% of the contact interval (Fig. 4). Patterns at the knee differ from those at other joints. Early in the step the GRF exerts a knee flexor moment that reaches a maximum at approximately 20% contact, earlier than maxima at other joints. This moment rapidly decreases, however, typically becoming an extensor moment after midstance, although the maximum flexor moment is typically two to three times greater than the maximum extensor moment (Fig. 4).

The GRF also exerts torsional moments on the femur (Fig. 4). As the GRF acts posterior to the femur throughout contact, it tends to exert a moment that would rotate the femur anteriorly or inwardly (i.e. counterclockwise if viewing the right femur from its proximal end). As the femur retracts and the hip moves forward, torsional moments increase to a maximum between 30% and 40% of the contact interval, similar to the timing of maximal hip and ankle moments. Moments are often maintained near their maximum for half or more of the stance phase (Fig. 4).

Femoral stresses

Because the GRF exerted a retractor moment throughout stance, contributions of retractor muscles to stresses on the posterior aspect of the femur appear inconsequential in our equilibrium-based model of bone loading (see Materials and methods, and Appendix). However, because of the large moments exerted by the GRF in the abductor direction at the hip, as well as about the other hindlimb joints, other hindlimb muscles appear to exert large forces that make substantial contributions to axial and bending stresses in the femur. Estimates of force exerted by the hip adductors and knee extensors (pulling in opposite directions) at peak tensile stress averaged 1.9±0.1 BW and 1.9±0.2 BW, respectively, across all four turtles. Hip adductor and knee extensor muscles act to bend the femur in opposite directions, with hip adductors placing the ventral surface in compression and knee extensors placing the dorsal surface in compression. However, to counter the combined knee flexor moments of the GRF and the ankle extensor muscles that span the knee joint (Blob and Biewener, 2001), knee extensor forces exceeded the forces exerted by hip adductors that span the midshaft of the femur (i.e. adductor femoris only, see Appendix)

in cooters, causing the net stress induced by muscles to be compressive on the dorsal aspect of the femur (Fig. 5). Bending stress induced by the axial component of the GRF due to bone curvature is very small, with little effect on overall bone loading (Fig. 5). External bending moments exerted by transverse components of the GRF on the anterior and dorsal surfaces of the femur are larger than those due to bone curvature (Fig. 5) but, for the dorsal femur, compressive stresses induced by limb muscles exceed those induced by the GRF.

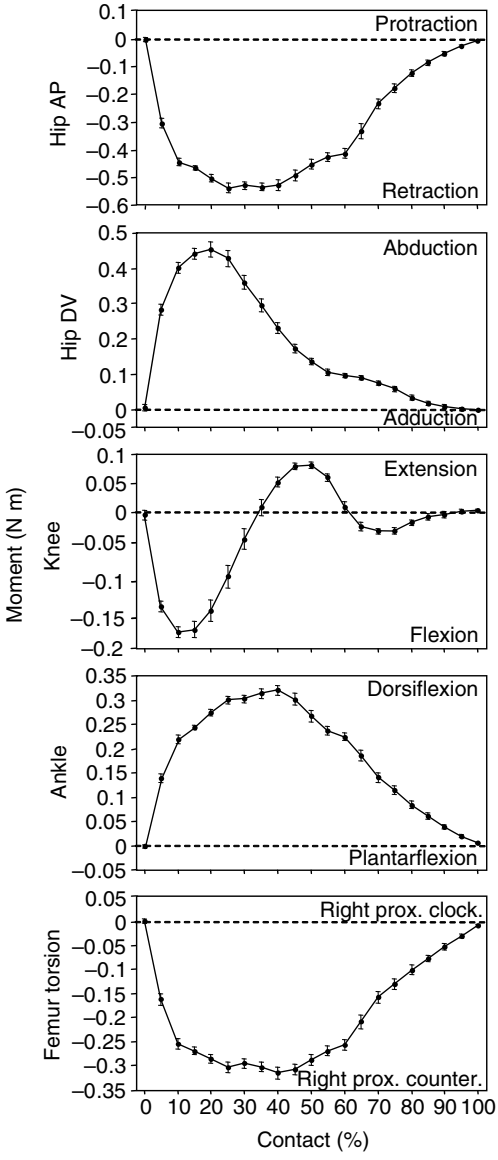

Fig. 4. Moments exerted by the GRF about the hindlimb joints and the long axis of the femur from an individual cooter. All plots show means (±s.e.m.) over *N*=20 trials. Note that axis scales differ for these plots to provide increased resolution for smaller moments. Directions of moments are labeled to the right of the figure plots. Hip AP, the GRF moment about the hip in the anatomical anterior and posterior directions; Hip DV, the GRF moment about the hip in the anatomical dorsal and ventral directions; Right prox. clock., torsional GRF moment, clockwise when viewing the right femur from the proximal end; Right prox. counter., torsional GRF moment, counterclockwise when viewing the right femur from its proximal end.

The femur of *P. concinna* is loaded in a combination of axial compression and bending, along with appreciable torsion. Maximum tensile and compressive stresses occurred nearly simultaneously during each step (Table 4). Although the timing of peak stress varied among individuals, it generally occurred prior to midstance, just in advance of the peak magnitude of the net GRF (at a magnitude of 0.35 BW *versus* 0.52 BW at peak net GRF), at a time when the GRF vector was oriented nearly vertically (Table 4; Fig. 6). The net plane of bending (i.e. neutral axis angle from the anatomical AP axis) shifts over the course of the step reflecting the axial rotation of the femur (Blob and Biewener, 1999; Blob and Biewener, 2001), but at the time of peak tensile stress (pooled mean: 36.6±3.2% contact) tended to place the anatomical 'anterior' cortex in tension and the 'posterior' cortex in compression (Fig. 6), somewhat similar to observations previously made in iguanas and alligators (Blob and Biewener, 2001). Because the GRF is essentially vertical for most of stance, shifting of the neutral axis indicates maintenance of a similar absolute direction of bending through the step.

Because axial compression (–3.5±0.1 MPa) is superimposed on bending during stance, peak compressive stresses are greater than peak tensile stress (Table 4). Peak tensile and compressive stresses averaged 24.9±1.0 MPa and –31.1±1.0 MPa, respectively, across all four turtles. Overall mean stresses were very similar to those reported for *I. iguana* (tensile: 27.1±2.1 MPa; compressive: –37.0±2.8 MPa) but somewhat higher than found for *A. mississippiensis* (tensile: 11.7±0.6 MPa; compressive: –16.4±0.9 MPa) (Blob and Biewener, 2001).

Shear stresses induced in the femur by GRF averaged 13.7±0.5 MPa across all four turtles (Table 4), considerably higher than shear stresses reported for either the femora or tibiae of *I. iguana* and *A. mississippiensis* (Blob and Biewener, 2001). These high shear stresses reflect the large rotational moment exerted by the GRF on the cooter femora, tending to produce inward rotation during stance.

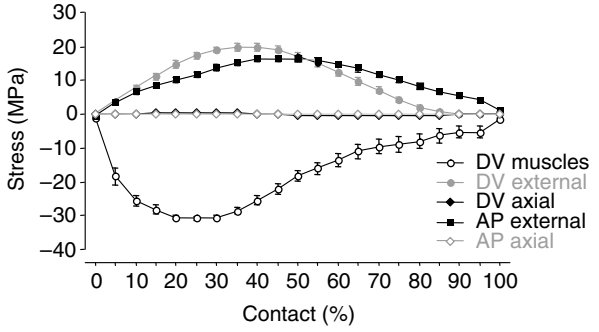

Fig. 5. Components of bending stress in the femur induced by muscles and GRF components from an individual cooter. All data are mean (±s.e.m.) stresses over *N*=21 trials. Stresses plotted are those occurring on the dorsal surface for forces acting to cause dorsoventral (DV) bending, and those occurring on the anterior surface for forces acting to cause anteroposterior (AP) bending. Tensile stress is positive and compressive stress is negative. 'Muscles' indicates stresses induced by major muscle groups in the direction indicated; 'external' indicates stresses induced by the GRF acting in the direction indicated; 'axial' indicates stresses induced by the axial component of the GRF due to bone curvature in the direction indicated. Bending stresses induced by axial forces are very small and overlap along the zero line for the DV and AP directions. Note that the retractor moment generated by the GRF for most of stance (Fig. 4) precludes calculation of muscular contributions to AP bending stress in the femur, but that resulting stress underestimation is minimized to the extent possible (see Appendix).

Table 4. Mean peak stresses for femora of *P. concinna* with GRF magnitudes and orientations at peak tensile stress

Individual	Peak stress				Peak tens. time (%)	Peak comp. time (%)	Neutral axis angle from AP (deg.)	Net GRF (BW)	GRF AP angle (deg.)	GRF ML angle (deg.)	Speed (CL s^{-1})
	Tensile (MPa)	Compressive (MPa)	Axial (MPa)	Shear (MPa)							
pc04 (*N*=20)	39.1±0.2	–44.7±0.2	–2.9±0.1	19.3±0.5	9.9±1.2	12.1±1.0	17.5±0.9	0.39±0.02	5.3±0.6	–13.2±0.5	0.7±0.10
pc05 (*N*=18)	15.9±0.8	–20.9±0.5	–3.2±0.1	12.7±0.6	63.3±5.7	62.9±5.7	48.3±10.4	0.27±0.04	3.2±2.7	–9.5±2.3	0.6±0.05
pc07 (*N*=21)	21.3±0.5	–26.5±0.5	–3.2±0.1	10.8±0.7	50.4±5.6	39.3±6.4	44.2±8.8	0.35±0.05	6.1±2.3	–12.2±1.5	0.9±0.10
pc08 (*N*=19)	22.2±0.5	–31.3±0.7	–4.7±0.1	11.9±0.4	24.2±3.7	22.2±2.7	24.3±2.2	0.39±0.02	8.1±0.5	–15.6±1.1	0.6±0.05
Mean ± s.e.m.	24.9±1.0	–31.1±1.0	–3.5±0.1	13.7±0.5	36.6±3.2	33.6±3.1	33.4±3.7	0.35±0.01	5.6±0.9	–12.7±0.8	0.7±0.03

Shear stresses are reported for counterclockwise rotation of the right femur as viewed from the proximal end.
Peak tension (tens.) and compression (comp.) time are shown as a percentage.
Deviations of the neutral axis from the anatomical anteroposterior (AP) axis of each bone are counterclockwise in direction (i.e. positive angle from horizontal at 0°).
CL, carapace length; ML, mediolateral.
Peak stresses were determined from force platform loading data; *N*=number of steps analyzed.
Values are means ± s.e.m.

As noted in Materials and methods, these values are minimum estimates that do not account for torsion induced by limb muscles.

Mechanical properties and safety factor calculations

P. concinna femora showed a high yield stress in bending, averaging 305.9±66.3 MPa, though tibiae showed considerably lower mean yield stresses (143.4±22.1 MPa; Table 5). These values are higher than failure stresses for Galápagos tortoise (*Geochelone midas*) femora reported by Currey (Currey, 1990), although his experiments were performed on extracted bone tissue specimens tested in unaxial tension, rather than whole bones tested in bending. Both femora and tibiae of cooters exhibited toughness during bending tests, with no bones fracturing catastrophically under high loads. *P. concinna* femora also showed yield stresses in torsion (78.1±6.6 MPa) that were higher than values reported for bovine and human bone [53–57 MPa (Currey, 2002)].

Because of the differing values of yield strength in bending for the femur and tibia in cooters, femoral safety factor calculations were based only on mechanical property data from the femur rather than on average values across the two hindlimb bones. Mean safety factor to yield in bending for the femur in *P. concinna* was 13.9 (Table 5), with a worst-case estimate that decreased to 2.8. A mean safety factor of approximately 14 is high compared with mean safety factors of 8.0 and 6.7 reported from force platform analyses of femoral loading for *I. iguana* and *A. mississippiensis*, respectively (Blob and Biewener, 2001). However, the worst-case estimate is lower than those reported for *I. iguana* and *A. mississippiensis*. Mean safety factor to yield in shear for the femur of *P. concinna* was 6.3 (Table 5), with a worst-case estimate that decreased to 3.1.

Correlations of loading parameters with peak tensile stress

One cooter had significantly higher femoral stresses than the other three individuals (ANOVA, $P<0.01$), causing values of its kinematic and force variables to cluster together and unduly influence evaluations of the significance of regressions of peak stress on kinematic and loading parameters. As a result, data from this individual were excluded from regression analyses, and evaluations of factors correlated with higher tensile stress in cooter femora were based on data from the $N=58$ trials for the remaining three individuals. Across these individuals, neither the speed of walking nor the AP or ML inclination of the GRF was significantly correlated with peak tensile stress magnitude, but higher stresses were correlated with higher magnitudes of the net GRF (Table 6). Peak tensile stresses were also correlated with several kinematic variables, as higher stresses tended to occur in steps in which the femur was held in a more protracted and adducted (depressed) orientation, and in which the knee was more flexed (Table 6). These kinematic correlations were reflected in several correlations with force variables as well. Steps with higher tensile stress tended to be ones in which the GRF had greater moment arms (normalized for carapace length) at the ankle and hip (consistent with the more protracted and adducted position of the femur in higher stress steps), and in which the ankle extensor, knee extensor and hip adductor muscles all exerted higher forces (normalized for body weight: Table 6).

Several kinematic and force parameters show correlations with high stress in iguanas that are similar to those in river cooters. For example, in iguanas peak tensile stress is correlated with peak GRF magnitude, but is not correlated with locomotor speed, or with AP or ML inclination of the GRF (Table 6). Among kinematic parameters, iguanas differ from cooters in that most limb position variables are not significantly correlated with higher tensile stress. However, iguanas do show a near significant ($P=0.069$) trend for tensile stresses to increase with more upright (i.e. adducted) posture (Blob and Biewener, 2001), as in cooters (Table 6); moreover, peak compressive stresses are significantly greater in more upright steps in iguanas (Blob and Biewener, 2001). Also similar to cooters, both ankle extensors and knee extensors exert higher forces in steps with

Table 5. Mechanical properties and safety factors for femora and tibiae of *P. concinna*

Bone	Bending			Torsion		
	N	Yield stress (MPa)	Safety factor mean	*N*	Yield stress (MPa)	Safety factor mean
Femur	3	305.9±66.3	13.9	3	78.1±6.6	6.3
Tibia	4	143.4±22.1	6.5*	–	–	–

*Tibial safety factor calculated from tibia yield stress and average peak locomotor stresses of the femur.
Yield stress values are means ± s.e.m.

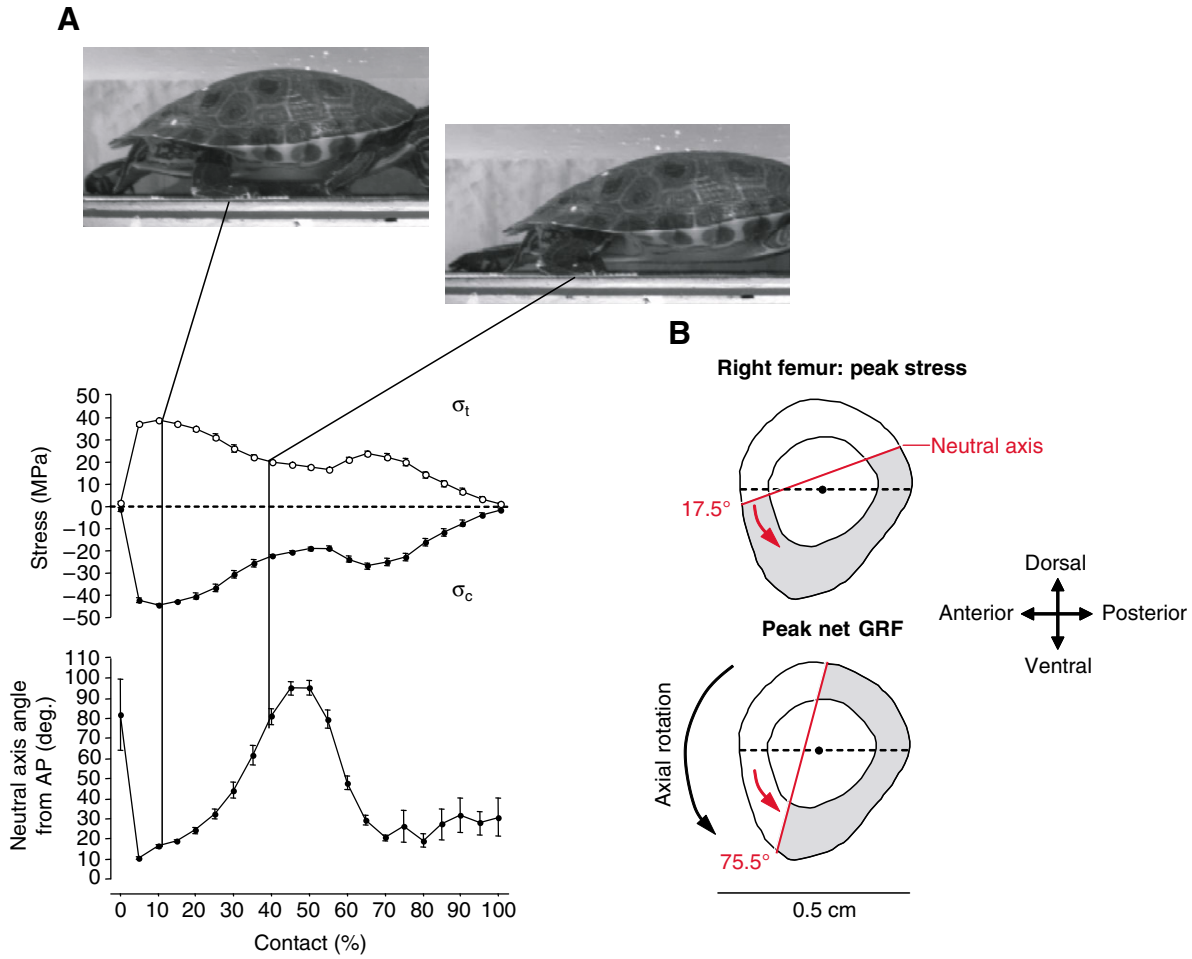

Fig. 6. (A) Maximum tensile (σ_t, open circles) and compressive (σ_c, filled circles) stresses acting in the right femur and neutral axis angle from the anatomical AP axis of the femur from an individual cooter. Plots show means (±s.e.m.) over *N*=20 trials. Frame stills show limb position at the time of maximum tensile stress (left image) and at the time of peak net GRF magnitude (right image). Solid vertical lines mark the relative timing of these loading events. (B) Schematic cross-sections of a right femur illustrating neutral axis orientations for bending (red line and values) at peak tensile stress (upper) and peak net GRF (lower). Neutral axis is illustrated offset from the centroid (dark circle) due to axial compression superimposed on bending loads. Mean rotation of the neutral axis >45° over the course of a walking step indicates that the 'posterior' cortex of the femur experiences compression (shaded) and the 'anterior' cortex experiences tension (unshaded), placing the plane of bending nearly parallel with the anatomical dorsoventral (DV) axis of the bone. The curved black arrow indicates the inward rotation of the femur during a step, which shifts the anatomical plane of bending to align more closely with the anatomical DV axis.

higher femoral stress in iguanas; however, unlike cooters the hip adductors do not (Table 6). Thus, in both cooters and iguanas, limb position (e.g. femoral abduction/adduction angle) and GRF magnitude have a stronger bearing on limb bone stress than GRF orientation.

DISCUSSION

Femoral loading regimes in river cooter turtles: the prevalence of torsion and comparisons with other taxa

Like iguanas and alligators, the other species of non-avian reptiles in which limb bone loading has been examined (Blob and Biewener, 1999; Blob and Biewener, 2001), the femur of river cooters is loaded in a combination of axial compression, bending and torsion. These loading regimes result from the combined action of muscular forces and a GRF that is directed nearly vertically for much of the step, including when femoral stresses are highest. Despite using a highly sprawled walking posture in which the femur is nearly parallel to the ground (Figs 1, 2 and 6), the mean medial inclination of the GRF at the time of peak tensile stress is only 12.7° in cooters (Table 4), confirming findings of a nearly vertical GRF from the only previous study of single limb forces in turtles (Jayes and Alexander, 1980) and similar to results from other reptiles [3–8° inclination (Blob and Biewener, 2001)] and even many mammals that use a more parasagittal posture (Biewener et al., 1983; Biewener et al., 1988). The similarity of GRF orientation at peak stress across these diverse taxa is striking, indicating that differences in bone loading patterns among these taxa, and potentially across tetrapods more broadly, depend more strongly on limb position and the orientation of the GRF relative to the femur than on the absolute orientation of the GRF.

A prominent similarity in femoral loading among cooters, iguanas and alligators is that the non-parasagittal kinematics of these species places their femora at large angles to the GRF. The mean angles observed at peak tensile stress in alligators (62.0±2.4°) and iguanas (74.0±3.3°) (Blob and Biewener, 2001) were actually exceeded in cooters such that the GRF and femur were nearly orthogonal (89.6±1.1°; Table 3). As a result, in all three reptilian groups, GRF components transverse to the femur generally exceed

Table 6. Results of regressions of peak tensile stress in the femur during locomotion on kinematic and force variables for *P. concinna* and *I. iguana*

	P. concinna				*I. iguana*			
Variable	RMA slope	*R*	*P*	*F*	RMA slope	*R*	*P*	*F*
FemTV angle (+) (deg.)	–0.17	0.44	0.001*	13.68	1.44	0.33	0.10	3.01
FemHZ angle (–) (deg.)	–0.57	0.35	0.01*	8.02	–0.97	0.36	0.07	3.61
Knee angle (+) (deg.)	–0.27	0.37	0.005*	8.61	–1.82	0.29	0.15	2.26
Ankle angle (+) (deg.)	0.21	0.11	0.43	0.62	–1.72	0.11	0.59	0.29
F_m kext (+) (BW)	3.29	0.36	0.01*	8.35	0.97	0.88	<0.0001*	82.40
F_m add (–) (BW)	–4.81	0.57	<0.0001*	26.94	–0.18	0.00	0.99	0.00
F_m aext (+) (BW)	4.69	0.65	<0.0001*	41.83	1.49	0.62	0.001*	15.26
R_{hip} (+) (CL)	48.99	0.29	0.03*	4.90	0.95	0.03	0.88	0.02
R_{knee} (–) (CL)	–74.53	0.24	0.07	3.37	0.51	0.35	0.08	3.31
R_{ankle} (+) (CL)	186.06	0.29	0.03*	5.08	–0.51	0.12	0.55	0.36
Net GRF (+) (BW)	20.42	0.48	0.0001*	17.06	0.04	0.74	<0.0001*	29.44
GRF AP angle (+) (deg.)	–0.49	0.05	0.71	0.14	1.07	0.20	0.32	1.04
GRF ML angle (–) (deg.)	–0.41	0.10	0.47	0.54	–0.65	0.14	0.48	0.51
Speed (+) (CL s^{-1})	–45.01	0.01	0.94	0.01	0.05	0.34	0.09	3.19

All force and kinematic variables were determined at the time of peak tensile stress.

*RMA slopes significant at $P<0.05$; $N=58$ for all *P. concinna* regressions; $N=26$ for all *I. iguana* regressions (data from Blob and Biewener, 2001).

Muscle force and moment arm data normalized for body weight (BW) and carapace length (CL), respectively, for *P. concinna* only.

FemTV, hip protraction/retraction angle; FemHZ, hip abduction/adduction angle; F_m, force exerted by a muscle group; kext, knee extensors; add, femoral adductors; aext, ankle extensors; *R*, moment arm of GRF about a limb joint; net GRF, magnitude of resultant GRF vector; GRF AP, anterioposterior angle of GRF vector (in direction of travel); GRF ML, mediolateral angle of GRF vector (orthogonal to direction of travel).

Positive variables (+): positive slopes indicate increasing values with increased stress; negative slopes indicate decreasing values with increased stress.

Negative variables (–): positive slopes indicate decreasing values with increased stress; negative slopes indicate increasing values with increased stress.

components acting along the femoral axis, producing much larger bending moments and stresses than those induced by axial forces as a result of bone curvature (Fig. 5). Although high transverse forces have been reported in small mammals using a crouched limb posture (Biewener, 1983a), they are not typical of large mammals using upright limb posture, in which bending induced by axial forces due to bone curvature is usually more substantial (Biewener et al., 1983; Bertram and Biewener, 1988; Biewener et al., 1988).

The prominence of torsion as a loading regime in cooter femora is also notable. Although torsion has been noted in the limb bones of walking birds such as chickens (Biewener et al., 1986; Carrano, 1998) and emus (Main and Biewener, 2007), it is typically less substantial among the quadrupedal mammals in which bone loading has been evaluated (Biewener, 1990; Biewener, 1991). However, torsional loading was quite high in the hindlimb bones of iguanas and alligators (Blob and Biewener, 2001), with shear strains exceeding bending strains (Blob and Biewener, 1999). Based on our analyses of locomotor forces, the significance of limb bone torsion appears to be even greater in turtles than in other non-avian reptiles. Differences in neutral axis orientation for cooters, *versus* alligators and iguanas, suggest that cooters rotate the femur to a greater degree (Fig. 6B). This orients the cooter femur in (absolute) space such that the anatomical anterodorsal surface is placed in tension in cooters, rather than the anatomical anteroventral surface that is in tension in alligators and iguanas (Blob and Biewener, 2001). Consistent with this considerable femoral rotation, shear stresses induced by the GRF (not accounting for muscular contributions) averaged almost 14 MPa across all four cooters (Table 4), over twice the magnitude of even the high average of 5.8 MPa calculated for the femur of iguanas (Blob and Biewener, 2001). In addition to femoral rotation, another factor potentially contributing to high shear stresses in cooters may be the articulation of the femur with a body axis made rigid by fusion to the shell. In other sprawling taxa such as lizards and crocodilians, lateral body undulations during locomotion may help to accommodate femoral twisting. With a rigid body axis in turtles, such torsional loads must be resisted strictly by the limb.

The large torsional stresses observed in cooters result from the GRF acting with a long moment arm tending to produce inward femoral rotation throughout the step (Fig. 4). Such high magnitudes of shear stress in turtle femora differ from the predictions of Reilly et al. (Reilly et al., 2005), who proposed that elevated torsional loading would only be expected in lineages that drag a heavy tail along the ground while walking or running. The tail of cooters (and most other turtle species) is quite short and does not reach the ground during walking, but they still exhibit some of the largest torsional stresses calculated for the limb bones of any terrestrial tetrapod. Thus, dragging of the tail, by itself, does not appear to be an overwhelming factor determining the orientation of the GRF and its tendency to rotate the femur during hindlimb contact. In alligators, although shear strains indicate an inward (medial) twisting of the femur, shear magnitudes are maximized early in the step, while the GRF induces an outward (lateral) torsional moment (Blob and Biewener, 2001; Reilly et al., 2005). This indicates that peak torsion in the femur of alligators is induced by contraction of the hip retractor caudofemoralis, which inserts on the ventral aspect of the femur, against the torsional moment of the GRF. In contrast, the presence of a consistent GRF moment throughout the step in cooters that would tend to rotate the femur inward (Fig. 4) indicates that torsion induced by contraction of limb retractor muscles in turtles (e.g. caudi-iliofemoralis; Fig. 1, Table 1) would accentuate torsion generated by GRF moments. Direct, *in vivo* measurements of limb bone strains on the cooter femur would, therefore, be expected to show high shear strains that would peak earlier in the step, when rotational moments of both the GRF and limb muscles would be maximal.

Bending magnitudes and mechanics in cooter femora: correlations with limb posture

Previous observations of locomotor forces and limb structure in turtles led to alternative expectations for the loads their limb bones

would experience. Although peak net GRF magnitudes acting on single turtle limbs were fairly low in previous studies [~0.5 BW (Jayes and Alexander, 1980)], the highly sprawled posture of turtles was expected to orient their limbs nearly perpendicular to the GRF, potentially elevating bending stresses. The combination of axial compression and bending that we calculated in river cooter turtles subjected their femora to peak stresses averaging 24.9 MPa (tensile) and –31.1 MPa (compressive). These stress magnitudes are comparable to values calculated for the femora of other non-avian reptiles, particularly iguanas (Blob and Biewener, 2001), which collectively are generally lower than values typically reported for the limb bones of birds and mammals (Biewener, 1983a; Biewener et al., 1988; Biewener, 1991). The relatively low magnitude of the peak net GRF acting on cooter limbs probably does contribute to the lower magnitudes of stress in their femur. GRF magnitudes measured from cooters (average 0.52 BW, maximum 0.35 BW at peak stress; Tables 3 and 4) match well with previous data from other turtle species (Jayes and Alexander, 1980), and are probably related to the consistent presence of at least three feet on the ground in turtles (Walker, 1971; Zug, 1971; Zug, 1972) as well as their generally slow walking speeds (0.7 CL s^{-1}; Table 4). Another factor that may help to moderate stresses in cooter femora is the short length of their limb bones. The bending moments applied by forces acting transverse to a limb bone are directly proportional to the length of that bone (Alexander, 1974; Wainwright et al., 1976; Biewener, 1983a; Blob and Biewener, 2001). A formal comparison of the scaling of turtle limb bone dimensions compared with body mass (Bertram and Biewener, 1990; Blob, 2000) has yet to be performed, but rough comparisons indicate that turtles have shorter limb bones at a given body mass than many generalized reptiles. For example, while data from Blob and Biewener (Blob and Biewener, 2001) show that a 1.98 kg alligator had a femur 61.5 mm long, the two turtles in this study with a body mass of 2 kg (pc04 and pc07) had femoral lengths 7.2–15.5% shorter, at 52.0 and 57.1 mm, respectively (Table 2). Although the short femora of turtles probably arose in response to selection for other functions (e.g. retraction into the protection of the shell), an additional consequence of such a design could be to help limit limb bending stress.

Although femoral stresses in cooters are low compared with those in many species, the highly sprawling posture exhibited by cooters may still elevate their femoral stresses. For example, alligators, like cooters, show peak net GRF magnitudes of ~0.5 BW; however, alligators have lower femoral stresses, averaging under 15 MPa in tension and under –20 MPa in compression (Blob and Biewener, 1999; Blob and Biewener, 2001). One factor contributing to this difference in stress may be that alligators typically exhibit less sprawling limb posture than cooters, such that the angle between the femur and GRF averages 62° in alligators (Blob and Biewener, 2001) rather than nearly 90° in cooters (an essentially orthogonal angle that would be expected to elevate bending stresses). However, such a relationship between limb bone stress and posture across these species would be at odds with expectations based on how femoral stress changes in reptiles as individual animals use different postures. In cooters, as in iguanas (Blob and Biewener, 2001) and alligators (Blob and Biewener, 1999), peak limb bone stresses (or strains for alligators) increase with the use of more upright posture (Table 6). Other factors correlated with higher femoral stress are also similar between cooters and iguanas, particularly increases in the net GRF magnitude and the forces exerted by ankle and knee extensor muscles (Table 6). However, cooters show a number of additional factors correlated with higher femoral stress that are not evident in iguanas; in particular, higher femoral stresses in cooters are found in steps with higher hip adductor muscle forces and a more protracted femur, which appears to increase the moment arm of the GRF about the hip (Table 6). Thus, although turtles appear to show associations between limb bone stress and limb posture generally similar to those of other reptiles, distinctive aspects of the body plan of turtles, for example the lack of hip adductors spanning the knee joint (Walker, 1973), may require these responses to be produced through different mechanisms.

Femoral safety factors in turtles: mechanical basis and implications for the evolution of limb bone design

Comparisons of peak locomotor stress magnitudes with mechanical property data from cooter femora produce yield-based, 'mean' safety factor calculations of 13.9 in bending and 6.3 in shear. Safety factors for bending in cooter femora are much higher than values previously calculated for mammals (Alexander, 1981; Biewener, 1983a; Biewener, 1993) as well as other reptiles; for example, 8.0 was the highest force platform-based value for iguanas (Blob and Biewener, 2001). Data for comparisons of safety factors in shear are much more limited (and based on *in vivo* strain data rather than force platform studies), but among species in which shear is prominent, cooter femora have similar safety factors to iguanas and alligators of 4.9 and 5.4, respectively (Blob and Biewener, 1999), and much higher safety factors than the humerus of flying pigeons [1.9 (Biewener and Dial, 1995)]. For bending, high femoral safety factors result from a combination of both relatively low locomotor stresses (noted above) and elevated yield strength in cooters. The mean yield stress value of nearly 306 MPa for the femur in bending is substantially higher than most ultimate strength values reported from whole bone tests across taxa ranging from salamanders to lizards, birds and mammals (Biewener, 1982; Erickson et al., 2002), though higher failure stresses have been measured in some frogs (Espinoza, 2000; Hudson et al., 2004). It seems unlikely that the high yield stress values we obtained for femora were simply an artifact of our testing protocol, because we obtained lower values for our test specimens of tibiae that were similar to previous data from turtle limb bones (Currey, 1990). In contrast to bending stresses, femoral shear stresses during walking were relatively high for cooters compared with other taxa; nonetheless, cooter femora still maintain a high margin of safety against torsional failure, with mean yield stresses in torsion (78.1 MPa) almost 40% greater than values reported for other species (Currey, 2002). Thus, although variation in the mechanical properties of limb bones has often been viewed as a minor factor in the evolution of tetrapod limb design (Erickson et al., 2002), variations present in some lineages appear to have a substantial impact on the functional capacities of their skeletal structures (Blob and Snelgrove, 2006).

Proximate causes for the high bending and torsional resistance of the femur in cooters, such as elevated mineralization, low porosity or collagen fiber arrangement (Currey, 1969; Currey, 1988; Riggs et al., 1993), have yet to be evaluated. But why might such high safety factors be maintained in turtles? Several possible advantages have been proposed for the high safety factors observed in other non-avian reptiles (Blob and Biewener, 1999). For example, because non-avian reptiles typically remodel their bones at a slower rate than birds or mammals (Enlow, 1969; de Ricqlès, 1975; de Ricqlès et al., 1991; Owerkowicz and Crompton, 1997), potentially leading to a low capacity for microdamage repair (Lanyon et al., 1982; Burr et al., 1985), high safety factors in reptiles such as turtles could help to limit the risk of limb bone fatigue failure (Carter et al., 1981; Blob and Biewener, 1999). High safety factors could also help to accommodate high variability in loading or skeletal mechanical

properties (Alexander, 1981; Lowell, 1985; Blob and Biewener, 1999). Both femoral loads and mechanical properties are potentially quite variable in turtle species. Although coefficients of variation for the magnitudes of limb bone loads during steady-state locomotion (i.e. treadmill or runway studies) are typically 8% or less in birds and mammals (Biewener, 1991), bending and shear stresses in cooter femora show higher coefficients of variation at 33% and 31%, respectively, similar to the variability seen in alligators and iguanas (Blob and Biewener, 1999). Other behaviors, such as mating or digging, could also add to variability in the forces to which turtle limb bones are exposed. In addition, like other reptiles including alligators (Wink and Elsey, 1986), female turtles resorb endosteal bone preferentially from the femur as a source of calcium during egg laying (Edgren, 1960; Suzuki, 1963). Such fluctuations in mineral content could have significant effects on limb bone mechanical strength.

Although natural selection is often interpreted as a primary factor regulating the magnitudes of biological safety factors, selecting against safety factors that either provide insufficient protection or are excessively costly to maintain (Alexander, 1981; Lanyon, 1991; Diamond and Hammond, 1992; Diamond, 1998), the suggestion that natural selection acts to optimize safety factors across lineages has also met with skepticism (Garland, 1998). The high limb bone safety factors seen in non-avian reptiles could, for example, be an incidental consequence of selection on other traits (e.g. bone surface area needed for muscle attachment), or reflect the retention of an ancestral trait for which costs were not so high as to be selected against through time (Lande and Arnold, 1983; Blob and Biewener, 1999). If limb bone safety factors were ancestrally high in amniotes (or all tetrapods), then the lower safety factors observed across birds and mammals may represent convergent evolution rather than a shared feature inherited from a common ancestor. Data on limb bone loading are needed from additional vertebrate lineages, particularly amphibians, to evaluate this possibility. Nonetheless, even if limb bone safety factors higher than those typical of birds and mammals were ancestral for tetrapods, the safety factor magnitudes we calculated for cooters suggest that turtle limb bones may be 'over-designed' to an even greater degree than those of other non-avian reptiles. Higher safety factors might be possible in turtle limb bones because locomotor energetic economy (e.g. mechanical energy recovery) is generally not significant to walking turtles (Zani et al., 2005), and the metabolic cost of moving over-designed limb bones and a massive shell at the slow speeds typical of turtles may not be high enough to be disadvantageous. Loading data from distal limb bones in turtles, like the tibia, would be interesting in this context, as higher bone mass is energetically more expensive to move when it is placed distally from the body (Alexander, 1997; Alexander, 1998), and mechanical property data suggest that cooter tibiae have lower mechanical reinforcement against failure than femora. More broadly, however, our data on limb bone loading and safety factors in river cooters indicate a greater diversity of bone loading patterns and resistance to loads than had been recognized based on previous studies of mammals, birds and even other non-avian reptiles. Extension of these comparisons to a broader phylogenetic and functional range of species should provide substantial insight into the relationship between limb bone loading and limb bone design through the evolution of tetrapods.

APPENDIX

In the anteroposterior (AP) direction, five main muscles are in anatomical positions suitable to act as primary femoral retractors during stance in river cooters: pubotibialis (PT), flexor tibialis internus (FTI), flexor tibialis externus (FTE), caudi-iliofemoralis (CF) and ishiotrochantericus (IT) (Walker, 1973). Electromyographic (EMG) data verify activity during limb retraction for FTI and FTE in closely related red-eared slider turtles [*Trachemys scripta* (Earhart and Stein, 2000; Gillis and Blob, 2001; Blob et al., 2008)], and in our dissections of *P. concinna*, PT was so closely associated with FTI that we considered them as a single muscle group. In other reptiles, EMG and electrical stimulation data have indicated the caudofemoralis [homologous to the caudi-iliofemoralis of turtles (Walker, 1973)] to be the primary femoral retractor (Snyder, 1962; Reilly, 1995; Gatesy, 1997; Reilly and Blob, 2003). In our model, all five muscles were considered capable of generating force to oppose protractor moments induced by the GRF, with FTI, PT and FTE potentially contributing to midshaft stresses because only these three muscles span the length of the femur. However, our force platform recordings indicated that the GRF had a retractor moment for almost all of stance (see Results, Fig. 4). Despite known EMG activity of these femoral retractors, our model could not estimate their contribution to femoral stress. Therefore, our model might underestimate AP stresses on the femur, but we believe this underestimation is minimal. First, although active, these retractor muscles may only exert low forces during sustained walking if the GRF also tends to retract the limb. This would be consistent with findings of lower intensity FTI activity on land than in water in turtles (Gillis and Blob, 2001; Blob et al., 2008). In addition, femoral retractors are unlikely to need to exert substantial force to oppose the action of femoral protractors that might be active to balance retractor moments at the hip, because the two largest muscles in anatomical positions to protract the limb, iliofemoralis and puboischiofemoralis internus (PIFI) (Walker, 1973), are inactive for the first two-thirds of stance in turtles (Gillis and Blob, 2001; Blob et al., 2008), when the GRF is greatest in magnitude. A third muscle potentially active to counter femoral retractor moments, the ambiens, spans the length of the femur (Walker, 1973); thus, the forces it exerts would tend to cancel out bending induced by FTI, PT and FTE in the opposite direction. The large size and force generating capacity of hindlimb retractors in turtles may be more critical when first initiating terrestrial locomotion, or during swimming behaviors (Gillis and Blob, 2001; Blob et al., 2008).

Forces acting on the femur in the dorsoventral (DV) direction are exerted by muscles that span the hip and knee. Anatomical analyses by Walker (Walker, 1973) and our own dissections indicate that two major muscles situated along the ventral aspect of the femur could act as adductors to counter the abductor moment exerted by the GRF through most of stance (Fig. 4): adductor femoris and puboischiofemoralis externus (PIFE). Although contraction by PIFE may help oppose the GRF moment, this muscle does not span the femoral midshaft and, thus, does not contribute to femoral bending stress. Therefore, the muscular contribution to femoral bending stress in the ventral direction was calculated strictly from the force exerted by the adductor femoris. This was estimated from the total force required to balance the abductor moment of the GRF based on the proportion of total adductor cross-sectional area (PIFE + adductor femoris; Table 1) for which adductor femoris was responsible. However, because the GRF exerts a flexor moment at the knee for much of stance (particularly when GRF magnitudes are maximal in the first half of the step), knee extensors on the dorsal aspect of the femur must also be active, bending the femur dorsally and opposing the bending imposed by adductor femoris. Anatomical analyses indicate two primary knee extensor muscles in turtles: femorotibialis and iliotibialis (Walker, 1973). EMG data verify activity of the femorotibialis during walking in the turtle *T. scripta*

(Earhart and Stein, 2000; Gillis and Blob, 2001; Blob et al., 2008), a close relative of the river cooter. Although iliotibialis activity has not been tested in turtles, this muscle is closely associated with femorotibialis and is at least sporadically active during stance in other reptiles [alligators (Gatesy, 1997; Reilly and Blob, 2003)].

In river cooters, three thigh muscles (FTI, PT and FTE) cross the ventral aspect of the knee and have the potential to augment the knee flexor moment of the GRF (Walker, 1973). In addition, two of the four ankle extensors, lateral gastrocnemius and flexor digitorum longus (FDL) originate from the distal femur and also span the knee, contributing to the knee flexor moment. Thus, just as in iguanas and alligators, the iliotibialis and femorotibialis must exert enough force to counter the sum of these moments in order to maintain equilibrium at the knee (Blob and Biewener, 2001). However, because iliotibialis crosses the hip dorsally and exerts a moment opposite to that produced by the adductors, there is no unique solution to calculate the forces exerted by these muscle groups.

To account for known co-activation of muscle groups and other complications to the extent possible, we modeled the force production of muscles spanning the knee and hip in cooters as follows, using approaches generally similar to those of Blob and Biewener (Blob and Biewener, 2001), but with modifications appropriate for turtles as required. (i) Muscle groups were assumed to act in the same anatomical plane throughout stance. Although a potential source of error in force calculations for some muscles originating from the hip, it is probably reasonable for several major muscles close to the femoral shaft (e.g. femorotibialis). This rule was modified for the retractors FTI, PT and FTE, for which the capacity to flex the knee was considered despite their disposition primarily on the posterior (rather than ventral) aspect of the femur. (ii) The fraction of retractor force contributing to the flexor moment at the knee was calculated as proportional to the fraction of total retractor cross-sectional area contributed by retractors spanning the knee. The flexor moment generated by these retractors was calculated as the product of this force and the weighted mean moment arm of the biarticular retractors at the knee. (iii) The force exerted by hip adductors was calculated as the force necessary to maintain equilibrium with the abductor moment of the GRF at the hip. This approach underestimates adductor force because it does not account for the abductor moment of iliotibialis at the hip; however, this effect is minimized because iliotibialis accounts for <25% of knee extensor cross-sectional area (and force exerted; Table 1). (iv) The knee flexor moment generated by the ankle extensors spanning the knee was calculated as the proportion of the total force needed to maintain equilibrium at the ankle exerted by lateral gastrocnemius and FDL (based on their cross-sectional area), multiplied by the weighted mean moment arm of these muscles at the knee. (v) Force of the knee extensors was calculated by dividing the total knee flexor moment by the weighted mean moment arm of the femorotibialis and iliotibialis muscles at the knee.

In some trials, muscle forces calculated for the knee extensors were extremely high and would have resulted in unreasonable muscle stresses. Maximum isometric stresses of reptilian limb muscle are generally over 200 kPa (John-Alder and Bennett, 1987; Marsh, 1988), though muscle stresses can be as much as 80% greater than maximum isometric stress during lengthening contractions (Cavagna and Citterio, 1974; Flitney and Hirst, 1978). Because the knee flexes in the first half of the contact interval (Fig. 2), eccentric contraction of the knee extensors is likely. To accommodate these conditions, we made a final assumption in our model that prevented calculated muscle forces from exceeding values that could produce muscle stresses over 390 kPa.

We thank K. Shugart for assistance with data analysis, G. Rivera for construction of the trackway, A. Rivera for help with figures, N. Espinoza for discussion throughout this study, D. Lee for mechanical insights into the turtle body axis, two anonymous reviewers for constructive advice on our manuscript, and S. Cirilo, S. Gosnell, T. Maie, M. Pruette, A. Rivera, G. Rivera and M. Wright for assistance during the course of the experiments and help with animal care. J. DesJardins (Clemson Bioengineering) provided access to and generous assistance with mechanical testing equipment, D. Lieberman (Harvard) provided software for measurement of limb bone cross-sectional geometry, J. Walker (University of Southern Maine) provided access to QuickImage and QuickSAND software, and S. Bennett (South Carolina Department of Natural Resources) coordinated scientific collecting permits. Support by NSF (IOB-0517340) and the Clemson Department of Biological Sciences is gratefully acknowledged.

REFERENCES

Alexander, R. McN. (1974). The mechanics of a dog jumping, *Canis familiaris*. *J. Zool. Lond.* **173**, 549-573.
Alexander, R. McN. (1981). Factors of safety in the structure of animals. *Sci. Prog.* **67**, 109-130.
Alexander, R. McN. (1997). A theory of mixed chains applied to safety factors in biological systems. *J. Theor. Biol.* **184**, 247-252.
Alexander, R. McN. (1998). Symmorphosis and safety factors. In *Principles of Animal Design* (ed. D. W. Weibel, C. R. Taylor and L. Bolis), pp. 28-35. Cambridge: Cambridge University Press.
Beer, F. P. and Johnston, E. R., Jr (1997). *Vector Mechanics for Engineers: Statics and Dynamics* (6th edn). Boston, MA: McGraw-Hill.
Bertram, J. E. and Biewener, A. A. (1988). Bone curvature: sacrificing strength for load predictability? *J. Theor. Biol.* **131**, 75-92.
Bertram, J. E. and Biewener, A. A. (1990). Differential scaling of the long bones in the terrestrial Carnivora and other mammals. *J. Morphol.* **204**, 157-169.
Biewener, A. A. (1982). Bone strength in small mammals and bipedal birds: do safety factors change with body size? *J. Exp. Biol.* **98**, 289-301.
Biewener, A. A. (1983a). Locomotory stresses in the limb bones of two small mammals: the ground squirrel and chipmunk. *J. Exp. Biol.* **103**, 131-154.
Biewener, A. A. (1983b). Allometry of quadrupedal locomotion: the scaling of duty factor, bone curvature and limb orientation to body size. *J. Exp. Biol.* **105**, 147-171.
Biewener, A. A. (1989). Scaling body support in mammals: limb posture and muscle mechanics. *Science* **245**, 45-48.
Biewener, A. A. (1990). Biomechanics of mammalian terrestrial locomotion. *Science* **250**, 1097-1103.
Biewener, A. A. (1991). Musculoskeletal design in relation to body size. *J. Biomech.* **24** Suppl. 1, 19-29.
Biewener, A. A. (1993). Safety factors in bone strength. *Calcif. Tissue Int.* **53** Suppl. 1, S68-S74.
Biewener, A. A. and Dial, K. P. (1995). *In vivo* strain in the humerus of pigeons (*Columba livia*) during flight. *J. Morphol.* **225**, 61-75.
Biewener, A. A. and Full, R. J. (1992). Force platform and kinematic analysis. In *Biomechanics – Structures and Systems: A Practical Approach* (ed. A. A. Biewener), pp. 45-73. New York: Oxford University Press.
Biewener, A. A. and Taylor, C. R. (1986). Bone strain: a determinant of gait and speed? *J. Exp. Biol.* **123**, 383-400.
Biewener, A. A., Thomason, J. J., Goodship, A. and Lanyon, L. E. (1983). Bone stress in the horse forelimb during locomotion at different gaits: a comparison of two experimental methods. *J. Biomech.* **16**, 565-576.
Biewener, A. A., Swartz, S. M. and Bertram, J. E. A. (1986). Bone modeling during growth: dynamic strain equilibrium in the chick tibiotarsus. *Calcif. Tissue Int.* **39**, 390-395.
Biewener, A. A., Thomason, J. J. and Lanyon, L. E. (1988). Mechanics of locomotion and jumping in the horse (Equus): *in vivo* stress in the tibia and metatarsus. *J. Zool. Lond.* **214**, 547-565.
Blob, R. W. (2000). Interspecific scaling of the hindlimb skeleton in lizards, crocodilians, felids and canids: does limb bone shape correlate with limb posture? *J. Zool. Lond.* **250**, 507-531.
Blob, R. W. (2001). Evolution of hindlimb posture in non-mammalian therapsids: biomechanical tests of paleontological hypotheses. *Paleobiology* **27**, 14-38.
Blob, R. W. and Biewener, A. A. (1999). *In vivo* locomotor strain in the hindlimb bones of *Alligator mississippiensis* and *Iguana iguana*: implications for the evolution of limb bone safety factor and non-sprawling limb posture. *J. Exp. Biol.* **202**, 1023-1046.
Blob, R. W. and Biewener, A. A. (2001). Mechanics of limb bone loading during terrestrial locomotion in the green iguana (*Iguana iguana*) and American alligator (*Alligator mississippiensis*). *J. Exp. Biol.* **204**, 1099-1122.
Blob, R. W. and Snelgrove, J. M. (2006). Antler stiffness in moose (*Alces alces*): correlated evolution of bone function and material properties? *J. Morphol.* **267**, 1075-1086.
Blob, R. W., Rivera, A. R. V. and Westneat, M. W. (2008). Hindlimb function in turtle locomotion: limb movements and muscular activation. In *Biology of Turtles* (ed. J. Wyneken, M. H. Godfrey and V. Bels), pp. 139-162. Boca Raton: CRC Press.
Burr, D. B., Martin, R. B., Schaffler, M. B. and Radin, E. L. (1985). Bone remodeling in response to *in vivo* fatigue microdamage. *J. Biomech.* **18**, 189-200.
Carrano, M. T. (1998). Locomotion of non-avian dinosaurs: integrating data from hindlimb kinematics, *in vivo* strains and bone morphology. *Paleobiology* **24**, 450-469.

Carrier, D. R., Heglund, N. C. and Earls, K. D. (1994). Variable gearing during locomotion in the human musculoskeletal system. *Science* **265**, 651-653.
Carter, D. R., Smith. D. J., Spengler, D. M., Daly, C. H. and Frankel, V. H. (1980). Measurement and analysis of *in vivo* bone strains on the canine radius and ulna. *J. Biomech.* **13**, 27-38.
Carter, D. R., Harris, W. H., Vasu, R. and Caler, W. E. (1981). The mechanical and biological response of cortical bone to *in vivo* strain histories. In *Mechanical Properties of Bone* (AMD Vol. 45) (ed. S. C. Cowin), pp. 81-92. New York: American Society of Mechanical Energy.
Cavagna, G. A. and Citterio, G. (1974). Effect of stretching on the elastic characteristics and the contractile component of frog striated muscle. *J. Physiol. Lond.* **239**, 1-14.
Cirilo, S. R., Hill, S., Espinoza, N. R. and Blob, R. W. (2005). Limb bone strain rates in divergent locomotor modes: turtles and frogs compared. *Integr. Comp. Biol.* **45**, 1119.
Claussen, D. L., Snashall, J. and Barden, C. (2004). Effects of slope, substrate, and temperature on forces associated with locomotion of the ornate box turtle, *Terrapene ornate. Comp. Biochem. Physiol.* **138A**, 269-276.
Currey, J. D. (1969). The mechanical consequences of variation in the mineral content of bone. *J. Biomech.* **2**, 1-11.
Currey, J. D. (1984). *The Mechanical Adaptations of Bones*. Princeton, NJ: Princeton University Press.
Currey, J. D. (1988). The effect of porosity and mineral content on the Young's modulus of elasticity of compact bone. *J. Biomech.* **21**, 131-139.
Currey, J. D. (1990). Physical characteristics affecting the tensile failure properties of compact bone. *J. Biomech.* **23**, 837-844.
Currey, J. D. (2002). *Bones. Structure and Mechanics*. Princeton, NJ: Princeton University Press.
Demes, B., Qin, Y. X., Stern, J. T., Larson, S. G. and Rubin, C. T. (2001). Patterns of strain in the macaque tibia during functional activity. *Am. J. Phys. Anthropol.* **116**, 257-265.
de Ricqlès, A. J. (1975). On bone histology of living and fossil reptiles, with comments on its functional and evolutionary significance. In *Morphology and Biology of Reptiles* (*Linnean Society Symposium Series, Number 3*) (ed. A. d'A. Bellairs and C. B. Cox), pp. 123-150. London: Academic Press.
de Ricqlès, A. J., Meunier, F. J., Castanet, J. and Francillon-Vieillot, H. (1991). Comparative microstructure of bone. In *Bone, Vol. 3, Bone Matrix and Bone Specific Products* (ed. B. K. Hall), pp. 1-78. Baca Raton: CRC Press.
Diamond, J. M. (1998). Evolution of biological safety factors: a cost/benefit analysis. In *Principles of Animal Design* (ed. D. W. Weibel, C. R. Taylor and L. Bolis), pp. 21-27. Cambridge: Cambridge University Press.
Diamond, J. M. and Hammond, K. A. (1992). The matches, achieved by natural selection, between biological capacities and their natural loads. *Experientia* **48**, 551-557.
Earhart, G. M. and Stein, P. S. (2000). Scratch-swim hybrids in the spinal turtle: blending of rostral scratch and forward swim. *J. Neurophysiol.* **83**, 156-165.
Edgren, R. A. (1960). A seasonal change in bone density in female musk turtles, *Sternothaerus odoratus* (Latreille). *Comp. Biochem. Physiol.* **1**, 213-217.
Enlow, D. H. (1969). The bones of reptiles. In *Biology of the Reptilia, I, Morphology A* (ed. C. Gans, A. d'A. Bellairs and T. S. Parsons), pp. 45-80. London: Academic Press.
Erickson, G. M., Catanese, J., III and Keaveny, T. M. (2002). Evolution of the biomechanical material properties of the femur. *Anat. Rec.* **268**, 115-124.
Ernst, C. H., Lovich, J. E. and Barbour, R. W. (1994). *Turtles of the United States and Canada*. Washington, DC: Smithsonian Institution Press.
Espinoza, N. (2000). Scaling of the appendicular musculoskeletal system of frogs (Order Anura): effects on jumping performance. PhD Dissertation, University of Chicago, USA.
Espinoza, N. and Blob, R. W. (2004). Diversity and evolution of terrestrial loading patterns in tetrapod limb bones. *J. Morphol.* **260**, 289.
Flitney, F. W. and Hirst, D. G. (1978). Cross-bridge detachment and sarcomere 'give' during stretch of active frog's muscle. *J. Physiol. Lond.* **276**, 449-465.
Furman, B. R. and Saha, S. (2000). Torsional testing of bone. In *Mechanical Testing of Bone and the Bone-Implant Interface* (ed. Y. H. An and R. A. Draughn), pp. 219-239. Boca Raton: CRC Press.
Garland, T., Jr (1998). Conceptual and methodological issues in testing the predictions of symmorphosis. In *Principles of Animal Design* (ed. D. W. Weibel, C. R. Taylor and L. Bolis), pp. 40-47. Cambridge: Cambridge University Press.
Gatesy, S. M. (1997). An electromyographic analysis of hindlimb function in *Alligator* during terrestrial locomotion. *J. Morphol.* **234**, 197-212.
Gillis, G. B. and Blob, R. W. (2001). How muscles accommodate movement in different physical environments: aquatic vs. terrestrial locomotion in vertebrates. *Comp. Biochem. Physiol.* **131A**, 61-75.
Hedges, S. B. and Poling, L. L. (1999). A molecular phylogeny of reptiles. *Science* **283**, 998-1001.
Hildebrand, M. (1976). Analysis of tetrapod gaits: general considerations and symmetrical gaits. In *Neural Control of Locomotion* (ed. R. M. Sherman, S. Grillner, P. S. G. Stein and D. G. Stuart), pp. 203-236. New York: Plenum Press.
Hill, R. V. (2005). Integration of morphological data sets for phylogenetic analysis of amniota: the importance of integumentary characters and increased taxonomic sampling. *Syst. Biol.* **54**, 530-547.
Hudson, N. J., Bennett, M. B. and Franklin, C. E. (2004). Effect of aestivation on long bone mechanical properties in the green-striped burrowing frog, *Cyclorana alboguttata. J. Exp. Biol.* **207**, 475-482.
Jayes, A. S. and Alexander, R. McN. (1980). The gaits of chelonians: walking techniques for very slow speeds. *J. Zool. Lond.* **191**, 353-378.
John-Alder, H. B. and Bennett, A. F. (1987). Thermal adaptations in lizard muscle function. *J. Comp. Physiol. B* **157**, 241-252.
Keller, T. S. and Spengler, D. M. (1989). Regulation of bone stress and strain in the immature and mature rat femur. *J. Biomech.* **22**, 1115-1127.
LaBarbera, M. (1989). Analyzing body size as a factor in ecology and evolution. *Annu. Rev. Ecol. Syst.* **20**, 97-117.
Lande, R. and Arnold, S. J. (1983). The measurement of selection on correlated characters. *Evolution* **37**, 1210-1226.
Lanyon, L. E. (1991). Biomechanical properties of bone and response of bone to mechanical stimuli: functional strain as a controlling influence on bone modeling and remodeling behavior. In *Bone, Vol. 3, Bone Matrix and Bone Specific Products* (ed. B. K. Hall), pp. 79-108. Boca Raton: CRC Press.
Lanyon, L. E., Goodship, A. E., Pye, C. J. and MacFie, J. H. (1982). Mechanically adaptive bone remodeling. *J. Biomech.* **15**, 141-154.
Lieberman, D. E., Pearson, O. M., Polk, J. D., Demes, B. and Crompton, A. W. (2003). Optimization of bone growth and remodeling in response to loading in tapered mammalian limbs. *J. Exp. Biol.* **206**, 3125-3138.
Lieberman, D. E., Polk, J. D. and Demes, B. (2004). Predicting long bone loading from cross-sectional geometry. *Am. J. Phys. Anthropol.* **123**, 156-171.
Lowell, R. B. (1985). Selection for increased safety factors of biological structures as environmental unpredictability increases. *Science* **228**, 1009-1011.
Main, R. P. and Biewener, A. A. (2004). Ontogenetic patterns of limb loading, *in vivo* strains and growth in the goat radius. *J. Exp. Biol.* **207**, 2577-2588.
Main, R. P. and Biewener, A. A. (2007). Skeletal strain patterns and growth in the emu hindlimb during ontogeny. *J. Exp. Biol.* **210**, 2676-2690.
Marsh, R. L. (1988). Ontogenesis of contractile properties of skeletal muscle and sprint performance in the lizard *Diposaurus dorsalis. J. Exp. Biol.* **137**, 119-139.
McArdle, B. H. (1988). The structural relationship: regression in biology. *Can. J. Zool.* **66**, 2329-2339.
Modesto, S. P. and Anderson, J. S. (2004). The phylogenetic definition of Reptilia. *Syst. Biol.* **53**, 815-821.
Owerkowicz, T. and Crompton, A. W. (1997). Effects of exercise and diet on bone-building: a monitor case. *J. Morphol.* **232**, 306.
Reilly, S. M. (1995). Quantitative electromyography and muscle function of the hindlimb during quadrupedal running in the lizard *Sceloporus clarkii. Zoology* **98**, 263-277.
Reilly, S. M. and Blob, R. W. (2003). Motor control of locomotor hindlimb posture in the American alligator (*Alligator mississippiensis*). *J. Exp. Biol.* **206**, 4327-4340.
Reilly, S. M., Willey, J. S., Biknevicius, A. R. and Blob, R. W. (2005). Hindlimb function in the alligator: integrating movements, motor patterns, ground reaction forces and bone strain of terrestrial locomotion. *J. Exp. Biol.* **208**, 993-1009.
Rest, J. S., Ast, J. C., Austin, C. C., Waddell, P. J., Tibbetts, E. A., Hay, J. M. and Mindell, D. P. (2003). Molecular systematics of primary reptilian lineages and the tuatara mitochondrial genome. *Mol. Phylogenet. Evol.* **29**, 289-297.
Rieppel, O. (2000). Turtles as diapsid reptiles. *Zool. Scr.* **29**, 199-212.
Rieppel, O. and Reisz, R. R. (1999). The origin and early evolution of turtles. *Annu. Rev. Ecol. Syst.* **30**, 1-22.
Riggs, C. M., Vaughn, L. C., Evans, G. P., Lanyon, L. E. and Boyde, A. (1993). Mechanical implications of collagen fibre orientation in cortical bone of the equine radius. *Anat. Embryol.* **187**, 239-248.
Rubin, C. T. and Lanyon, L. E. (1982). Limb mechanics as a function of speed and gait: a study of functional strains in the radius and tibia of horse and dog. *J. Exp. Biol.* **101**, 187-211.
Snyder, R. C. (1962). Adaptations for bipedal locomotion in lizards. *Am. Zool.* **2**, 191-203.
Stein, P. S. G. (2003). Neuronal control of turtle hindlimb motor rhythms. *J. Comp. Physiol. A* **191**, 213-239.
Suzuki, H. K. (1963). Studies on the osseous system of the slider turtle. *Ann. N. Y. Acad. Sci.* **109**, 351-410.
Wainwright, S. A., Biggs, W. D., Currey, J. D. and Gosline, J. M. (1976). *Mechanical Design in Organisms*. Princeton: Princeton University Press.
Walker, J. A. (1998). Estimating velocities and accelerations of animal locomotion: a simulation experiment comparing numerical differentiation algorithms. *J. Exp. Biol.* **201**, 981-995.
Walker, W. F., Jr (1971). A structural and functional analysis of walking in the turtle, *Chrysemys picta marginata. J. Morphol.* **134**, 195-214.
Walker, W. F., Jr (1973). Locomotor apparatus of Testudines: the pelvic apparatus. In *Biology of the Reptilia, Vol. 4, Morphology D* (ed. C. Gans and T. S. Parsons), pp. 53-100. London: Academic Press.
Willey, J. S. and Blob, R. W. (2004). Tail kinematics of juvenile common snapping turtles during aquatic walking. *J. Herpetol.* **38**, 360-369.
Willey, J. S., Biknevicius, A. R., Reilly, S. M. and Earls, K. D. (2004). The tale of the tail: limb function and locomotor mechanics in *Alligator mississippiensis. J. Exp. Biol.* **207**, 553-563.
Wink, C. S. and Elsey, R. M. (1986). Changes in femoral morphology during egg-laying in *Alligator mississippiensis. J. Morphol.* **189**, 183-188.
Zani, P. A., Gottschall, J. S. and Kram, R. (2005). Giant Galápagos tortoises walk without inverted pendulum mechanical-energy exchange. *J. Exp. Biol.* **208**, 1489-1494.
Zardoya, R. and Meyer, A. (2001). The evolutionary position of turtles revised. *Naturwissenschaften* **88**, 193-200.
Zug, G. R. (1971). Buoyancy, locomotion, morphology of the pelvic girdle and hindlimb, and systematics of cryptodiran turtles. *Misc. Publ. Mus. Zool. Univ. Michigan* **142**, 1-98.
Zug, G. R. (1972). Walk pattern analysis of cryptodiran turtle gaits. *Anim. Behav.* **20**, 439-443.